11

Ultrafast charge carrier dynamics in organic (opto)electronic materials

H. DIESINGER, E. A. CHAN, J. YIN and C. SOCI,
Nanyang Technological University, Singapore

DOI: 10.1533/9780857098764.2.318

Abstract: The chapter is a summary of ultrafast time-resolved pump-probe spectroscopy techniques for the study of charge carriers in organic semiconductors. Four methods featuring sub-nanosecond time resolution are distinguished according to their probe wavelength: infrared active vibrational (IRAV) mode spectroscopy, time-resolved THz spectroscopy (TRTS), time-resolved microwave conductivity (TRMC), and transient photocurrent (TPC) spectroscopy. Examples of the application of these techniques to the study of charged photoexcitations in molecular crystals, pristine polymers and polymer donor–acceptor blends are presented. Presently accepted knowledge gathered with these methods is summarized, and the aptitude of each method for discriminating between free and localized charge carriers is discussed in view of its implication in the design and optimization of materials for organic photovoltaic devices.

Key words: infrared active vibrational (IRAV) modes, transient photocurrent (TPC) spectroscopy, time-domain terahertz spectroscopy (TRTS), time-resolved microwave conductance (TRMC).

11.1 Introduction

The nature of primary photoexcitations in organic semiconductors, particularly in conjugated polymers, has been the subject of an active debate in the scientific community for more than three decades (Sariciftci, 1997). The mechanisms of charge carrier photogeneration and thermalization promptly after photoexcitation are indicative of the strength of electron–electron interactions relative to the bandwidth (as manifested by the exciton binding energy), while carrier transport, trapping, and recombination processes are intimately related to the degree of order, purity, and morphology of the materials. Besides their fundamental interest, these processes determine the overall efficiency of organic electronic devices, such as organic photovoltaic cells; as such, there has been a lot of effort to develop charge-specific ultrafast techniques to probe their dynamics. Non-resonant probing spectroscopic methods allow the characterization of charged excitations (e.g. polarons) in organic semiconductors (for a discussion on ultrafast

probes of excitonic species see Chapter 10). In general, they rely on either all-optical or electro-optical techniques where charge carriers are photogenerated with an ultrashort (~100 fs) pump pulse and their dynamics is detected with a delayed probe. We limit this summary to a choice of techniques that: (i) are highly selective to charge carrier density and dynamics (i.e., we do not consider photoinduced absorption measurements probing the visible to near-infrared spectral region where polaronic signatures overlap with excitonic features); (ii) have temporal resolution between nanoseconds and femtoseconds, that is the timescale most relevant to study photogeneration and prompt recombination processes which are indicative of intrinsic electronic and transport properties; (iii) can discriminate between charge carriers with different degrees of localization. The techniques presented here operate at distinct probe wavelengths: infrared active vibrational (IRAV) modes are probed in the medium infrared optical region, time-resolved terahertz spectroscopy, or TRTS (also referred to as optical-pump terahertz-probe spectroscopy) detects carrier signatures in the far-infrared, time-resolved microwave conductivity (TRMC) is a contactless conductance probing method that uses free space radiation at a specific microwave frequency, whereas transient photocurrent (TPC) spectroscopy consists in detecting photocurrent transients in a waveguide configuration, covering a spectral range from direct current (DC) to upper microwave frequencies.

As the field of organic semiconductors evolved through the initial fundamental studies of molecular crystals to the more application-oriented investigation of conjugated polymers, donor-acceptor and hybrid organic–inorganic systems, these techniques have been widely employed toward the experimental characterization of the charge generation and transport properties of new materials and material combinations. In the early days, polydiacetylene has been widely considered as a model system for highly ordered organic semiconductors, where the availability of high-quality single crystal allowed the observation of intrinsic material properties with limited influence of trapping. The temperature and field dependence of the peak transient photocurrent measured at about 100 ps after photoexcitation have shown the need for modifying the assumption that carrier generation in low-mobility semiconductors is limited by geminate recombination (Moses *et al.*, 1987, 1989). As experimental techniques with higher time resolution and materials with less disorder became available, the charge carrier generation and transport behavior observed in the polydiacetylene model system was found to be of general validity for the whole class of low-mobility semiconductors. A classical example of highly ordered conjugated polymer system is stretch-oriented poly(*para*-phenylene vinylene), or PPV. In this system photogeneration and transport are greatly enhanced compared with amorphous PPV films, and carrier dynamics can be studied

on an extended timescale. Polarons and excitons in PPV were shown to be independent primary excitations by IRAV spectroscopy and fast TPC measurements (Soci *et al.*, 2005). Further studies of this system by TPC under high fluence showed that the initial photogeneration dynamics is dominated by bimolecular recombination, whereas the photocurrent tail that persists for a long time after photoexcitation is explained by a combination of bimolecular recombination, by recombination with trapped charges, and by trapping itself (Soci *et al.*, 2005). Geminate recombination is unnecessary to interpret the carrier dynamics.

The availability of ultrafast, all-optical probing techniques such as femtosecond optical-pump THz-probe allowed the experimental proof of direct polaron generation in a variety of organic semiconductors. The work by the groups of Hegmann and Ostroverkhova confirmed that, within the picosecond timescale, the initial photoconductance peak in ordered molecular crystals pentacene, tetracene and rubrene is field-independent and increases at low temperature, indicative of bandlike transport.

Recent studies of charged photoexcitations were mainly focused on low-bandgap polymers with a particular high yield of direct polaron generation, such as regioregular poly(3-hexylthiophene), rr-P3HT. P3HT was studied at timescales up to hundreds of nanoseconds by time-resolved microwave conductivity, the response of which is mostly determined by the Q-factor of the microwave resonance cavity containing the sample to typically 40 nanoseconds (De Haas and Warman, 1982). Although this method is too slow to resolve initial free-carrier photogeneration, it still allows monitoring the temperature dependence of the peak intensity. Temperature-dependent pulse-radiolysis TRMC of P3HT films with different molecular weight (MW) revealed positive temperature dependence of the conductivity that was more pronounced on medium MW films than on high MW ones. Since it was known that the conductivity of the material increases upon heating to the melting point and the increase of phoconductivity was observed below the melting point, the observed temperature dependence was assigned to a 'pre-melting' effect. Optical-pump THz probe spectroscopy featuring picosecond time resolution was also used to compare the complex carrier mobilities of a PPV derivative, poly(2-methoxy-5(2′-ethylhexyloxy)*p*-phenylene vinylene) (MEH-PPV), and rr-P3HT films (Hendry *et al.*, 2006). The study revealed that in P3HT, a real component of the photoconductivity, attributed to free charges, was still present after 150 ps, while in PPV the purely imaginary photoconductivity could be attributed to exciton polarizability.

Low-bandgap polymers blended with fullerene derivatives play a key role in solar energy conversion in polymer solar cells. In so-called bulk heterojunction systems, the photoexcited polymer absorber serves as

electron donor, and charge transfer toward the fullerene acceptor takes place at ultrafast ($t \sim 50$ fs) time scales. This process leads to extremely efficient charge separation, as first demonstrated by Sariciftci *et al.* (1992) using photoinduced absorption (PIA) and light-induced electron spin resonance (LESR). Photoluminescence is quenched by adding the fullerene acceptors, whereas a turnover in the PIA spectrum indicates a transition from stimulated emission to photoinduced absorption. More direct evidence was given by an ESR spectrum that showed the occurrence of ionic radicals. In 2001 Brabec *et al.* studied the dynamics of charge separated state generation by time-resolved PIA, observing both the excitonic stimulated emission band and the polaronic absorption band on a femtosecond timescale. The decay dynamics of the excitonic charge transfer state has recently been studied by a 'pump-push' technique (Bakulin *et al.*, 2012). The charge separated state increases photocurrent yield and slows down recombination, so that the slow carrier recombination time makes it accessible to all three methods (Soci *et al.*, 2005): TRTS, TRMC, and TPC. Pristine polymers and their blends were compared by transient photocurrents, showing an increase of the photocurrent decay timescale from 100 ps to some nanoseconds due to decreased recombination after the charge separation (Murthy *et al.*, 2012). Drude-like transport models (Cunningham and Hayden, 2008) and transport models involving barriers and wells (Nemec *et al.*, 2009) have been derived from optical-pump THz-probe experiments. Energy levels of traps in these systems were obtained from TRMC measurements (Savenije *et al.*, 2011). Such models reveal the existence of a distribution of carriers that are mobile on different length scales, which has tremendous importance for photovoltaic and photodetecting devices.

The organization of this chapter will loosely follow the material-driven research path highlighted above for the study of charged photoexcitations in organic semiconductors: Sections 11.2 to 11.5 are dedicated to the spectroscopic methods IRAV, TPC, TRTS, and TRMC, respectively; in each of these sections the principles and development of the spectroscopic method is first introduced, followed by its application to the study of organic crystal model systems, pristine polymers, and polymer donor–acceptor blends where applicable. The characteristic time resolution and the timescale of typical observation intervals of these methods are also summarized at the end of each Section. Section 10.6 puts emphasis on the extent of carrier localization and the aptitude of each of the methods presented to detect charge carriers that are free to contribute to galvanic currents or localized to a certain degree. To conclude, Section 10.7 summarizes generally accepted knowledge on photoexcitation, charge carrier conduction, trapping, and decay mechanisms in organic semiconductors.

11.2 Infrared-active vibrational (IRAV) modes

The pristine π-conjugated polymer chain is neutral and has a set of Raman-active vibrations that are strongly coupled to the electronic states. When introduced onto the backbone of a conjugated polymer either by chemical doping or photoexcitation, charge carriers (solitons, polarons and bipolarons) break the local symmetry and thereby transform the even parity Raman-active vibrational modes into odd-parity IRAV modes. These IRAV modes are distinguished from conventional IR-active modes in organic polymer by having a one-to-one correspondence with the strongest Raman-active modes of the polymer, as observed in resonant Raman scattering (Raman modes are referred to as 'amplitude modes'). The observation of IRAV modes indicates (Heeger *et al.*, 2010): (i) the existence of local structural distortion; (ii) the self-localization of charges; (iii) the strong coupling between self-localized charges and the local chain distortion. IRAV modes describe charge oscillations along the polymer chain (hence are also denoted as 'phase modes') and show unusually large oscillator strength. Their intensity is proportional to the charge carrier density induced (either by chemical, photo, or interfacial doping) on the polymer chain; therefore IRAV modes provide a unique probe for charge carrier density and dynamics in conjugated polymers. The first successful theoretical model for IRAV 'phase modes' was developed by Horovitz and colleagues (Horovitz, 1982). This model included effects of disorder, which inhibits electronic motion along the polymer chain, assuming a restoring force due to a 'pinning' potential. Introduction of the pinning potential renormalizes the bare frequencies of the skeleton chain and allows key properties of the IRAV modes to be derived, including their frequency (and the higher-frequency of IRAV modes induced by chemical doping compared to photo-doping), the one-to-one correspondence with even parity Raman modes, and their oscillator strength and relative intensities.

11.2.1 Experimental observations of IRAV modes in conjugated polymers

The first experimental observation of IRAV modes was made in doped polyacetylene, trans-(CH)x and trans-(CD)x , as shown in Fig. 11.1. Fincher and coworkers (Fincher *et al.*, 1979) found that upon doping two new absorption modes (1370 and 900 cm^{-1}) appeared in the IR region. The spectra were correctly attributed to molecular vibrations made IR-active by doping, and were considered an evidence for charged solitons.

In a later experiment, for doped polyacetylene the lowest frequency IRAV mode was found at approximately 900 cm^{-1} whereas upon photoexcitation the lowest frequency mode was at approximately 450 cm^{-1}

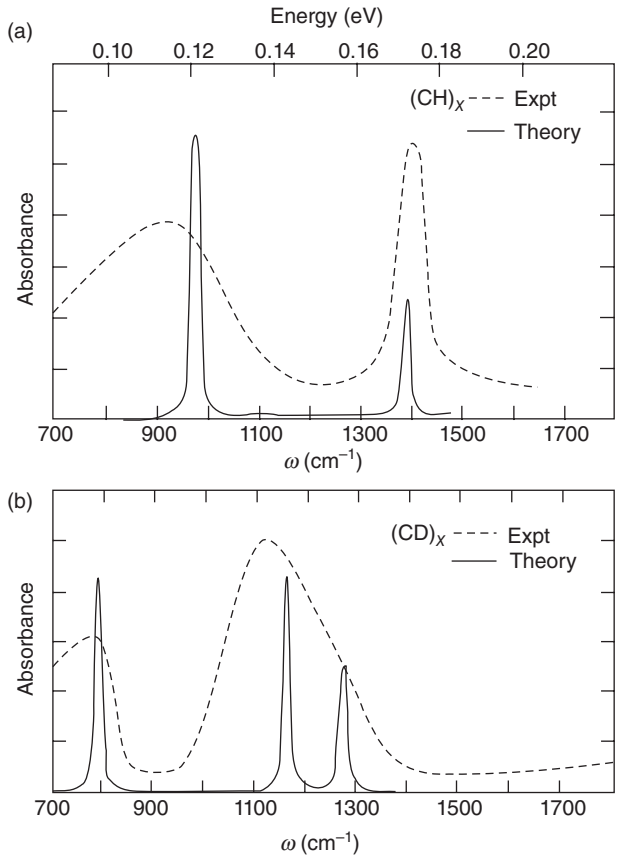

11.1 Doping-induced IRAV modes for *trans*-polyacetylene (a) *trans*-$(CH)_x$; (b) *trans*-$(CD)_x$. Reprinted with permission from Etemad, S., Pron, A., Heeger, A. J., Macdiarmid, A. G., Mele, E. J. & Rice, M. J. 1981. Infrared-active vibrational modes of charged solitons in $(CH)_x$ and $(CD)_x$. *Physical Review B*, **23**, 5137–5141. Copyright (1981) by the American Physical Society (DOI: 10.1103/PhysRevB.23.5137).

(Schaffer *et al.*, 1987). For doping-induced charged solitons, pinning arises from a combination of the coulomb attraction of the counter-ion and structural disorder. For photoinduced solitons the weaker pinning arises only from structural disorder due to the absence of translational symmetry.

Four localized IRAV modes (1088, 1161, 1200, 1354 cm^{-1}) associated with bipolaron distortions of the poly(3-hexylthiophene) (P3HT) chains and made infrared-active through coupling to the uniform translation of the bipolaron (see Fig. 11.2) were observed in both the doping-induced and PIA spectra, as for instance in polythiophene (PT) and P3HT (Kim *et al.*, 1988). An additional mode (1396 cm^{-1}) was identified from an IR-active

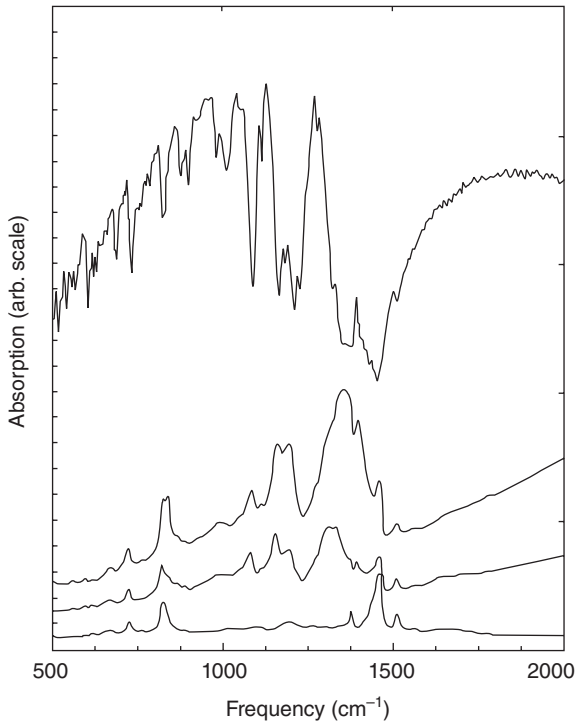

11.2 Detailed photoinduced infrared spectral changes of P3HT (top), and doping-induced infrared spectral changes of P3HT (bottom, undoped; second and third from bottom, 1 and 3 mol/% PF6-, respectively). Reprinted with permission from Kim, Y. H., Spiegel, D., Hotta, S. & Heeger, A. J. 1988. Photoexcitation and doping studies of poly(3-hexylthienylene). *Physical Review B*, **38**, 5490–5495. Copyright (1988) by the American Physical Society (DOI: 10.1103/PhysRevB.38.5490).

localized mode associated with the nonuniform translation of the bipolaron. Comparison of the energies of the photoinduced and doping-induced electronic transitions yields an estimate of the change in Coulomb energy of the bipolaron on photoexcitation, $U_B \approx 0.25$ eV; this relatively small value of U_B is consistent with bipolaron formation in P3HT.

11.2.2 Carrier density and dynamics investigated by ultrafast photoinduced IRAV modes absorption in conjugated polymers

In doped conjugated polymers, the strength of the IRAV modes is proportional to the doping level. Upon photoexcitation of semiconducting

polymers (Fincher *et al.*, 1979; Voss *et al.*, 1991), there is a one-to-one correspondence between the photoinduced IRAV modes (steady-state and transient) and the doping-induced IRAV modes of the same polymers (Fincher *et al.*, 1979; Voss *et al.*, 1991; Soos *et al.*, 1994; Ehrenfreund and Vardeny, 1997). Thus, the strength of the photoinduced IRAV modes is directly proportional to the density of photogenerated charge carriers on the polymer chain.

The first utilization of photoinduced IRAV modes for measuring photocarrier density was reported by Mizrahi and coworkers (Mizrahi *et al.*, 1999) for MEH-PPV/C60. With a temporal resolution on the order of 100 ps, they demonstrated PIA with the characteristic signatures of the IRAV modes, identical to those observed in steady-state experiments. Moses *et al.* (2000) utilized an approach for quantitatively estimating the density of photoinduced charge carriers at subpicosecond times by transient excited-state absorption probed in the spectral region spanning IRAV modes in the prototypical luminescent polymers, PPV and MEH-PPV (see Fig. 11.3). In MEH-PPV, the lifetime of the photoinduced IRAV modes and the exciton lifetime are different; the IRAV lifetime is more than an order of magnitude shorter than the lifetime of the neutral excitons as inferred from the photoluminescence decay time (Sariciftci *et al.*, 1992; Sariciftci and Heeger, 1994). When mixed with acceptors such as C60, conjugated polymers (PPV, MEH-PPV, etc.) undergo ultrafast photoinduced electron transfer with an

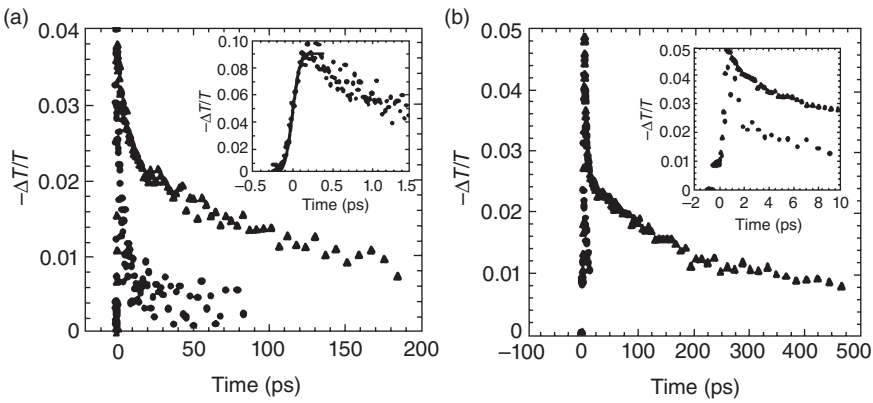

11.3 (a) Comparison of the PIA waveform in MEH-PPV and MEH-PPV/C60 (50%, C60, by weight), when pumped at the same light intensity at 800 nm and probed at 7 μm. (b) Comparison of the PIA waveform in MEH-PPV and MEH-PPV/C60 (10%, C60, by weight), when pumped at the same light intensity at 400 nm and probed at 9 μm. Reprinted with permission from Moses, D., Dogariu, A. & Heeger, A. J. 2000. Ultrafast photoinduced charge generation in conjugated polymers. *Chemical Physics Letters*, **316**, 356–360. Copyright (2000) by Elsevier (DOI: 10.1016/s0009-2614(99)01316-0).

associated increase in the PIA (both steady-state and transient) (Sariciftci *et al.*, 1992; Sariciftci and Heeger, 1994) and the photoconductivity signals (Lee *et al.*, 1993; Kraabel *et al.*, 1996), with an associated decrease (quenching) of the photoluminescence. As expected for photoinduced electron transfer, the strength of the photoinduced IRAV modes is proportional to the concentration of C60 in polymer/C60 composites. These observations provide direct experimental evidence that neutral excitons do not generate IRAV mode absorption. If excitons did generate IRAV mode absorption, addition of C60 would reduce the strength of the photoinduced IRAV modes, since the exciton density is quenched by efficient photoinduced electron transfer. In contrast, a significant increase in the IRAV mode PIA signal is measured upon addition of C60. So it is concluded that the strength of the photoinduced IRAV mode absorption provides a direct, all-optical, ultrafast probe to the charge carrier density at the short timescales ($t < 100$ fs) typical of carrier thermalization in disordered semiconductors.

Miranda *et al.* (2001) detected charged photoexcitations (polarons) in conjugated luminescent polymers by ultrafast photoinduced IRAV absorption. Figure 11.4 shows the spectra of the IRAV modes obtained with steady-state excitation for the MEH-PPV/C60 blend, and with the ultrafast setup for both MEH-PPV and the MEH-PPV/C60 blend. The steady-state and ultrafast spectra are in reasonable agreement, with all the spectral features present in both. They are also in good agreement with the data obtained at 100 ps time resolution. The ultrafast photoinduced IRAV modes demonstrate that polarons are produced in less than 100 fs, consistent with the early predictions of Su and Schrieffer. From the ratio of IRAV signals in pristine MEH-PPV and the MEH-PPV/C60 blend, the quantum efficiency for charge pair generation in pristine MEH-PPV when pumped at 400 nm was estimated as 10%.

Soci *et al.* (2005) studied the charge carrier density in highly ordered PPV by means of photoinduced absorption probed at IRAV modes. Figure 11.5 shows the intensity dependence of the IRAV signal, as obtained with pump polarized perpendicular and probe polarized parallel to the polymer chain axis. The ultrafast onset of the IRAV signals confirms that charge-carrier photogeneration happens on a time scale faster than the experimental resolution (300 fs). However, by taking into account the laser photon energy, intensity, laser beam size, reflectivity, and absorption coefficient of the sample, and assuming a carrier quantum yield of 10% (according to Miranda *et al.*), an absolute value for the initial carrier density consistent with direct fast transient photocurrent measurements was deduced.

Holt *et al.* (2009) used a variety of optical probes to study the long-lived photoexcitations in blends of MEH-PPV with a strong electron acceptor molecule, 2,4,7-trinitro-9-fluorenone (TNF). They found a strong PIA signal when the MEH-PPV/TNF blend is pumped using excitation below the

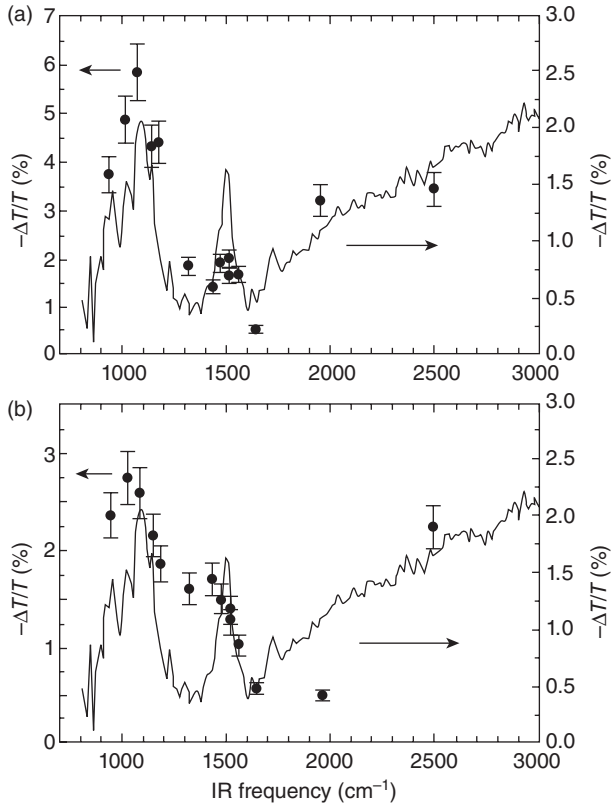

11.4 Photoinduced IRAV spectrum for (a) MEH-PPV/C60 blend and (b) pristine MEH-PPV. Reprinted with permission from Miranda, P. B., Moses, D. & Heeger, A. J. 2001. Ultrafast photogeneration of charged polarons in conjugated polymers. *Physical Review B*, **64**, 081201(R). Copyright (2001) by the American Physical Society (DOI: 10.1103/PhysRevB.64.081201).

pristine MEH-PPV bandgap. Fourier transform infrared (FTIR) spectroscopy PIA reveals the existence of various IRAV modes below 0.2 eV. The IRAV transitions indicate that P1 (0.3 eV) and P2 (1.2 eV) PIA bands are associated with charge species and confirm that charges indeed develop along the polymer backbone upon photoexcitation.

11.3 Transient photocurrent (TPC) spectroscopy

11.3.1 Auston switch

In 1975, D.H. Auston proposed a device for 'Picosecond optoelectronic switching and gating in silicon' (Auston, 1975). The principle was to create,

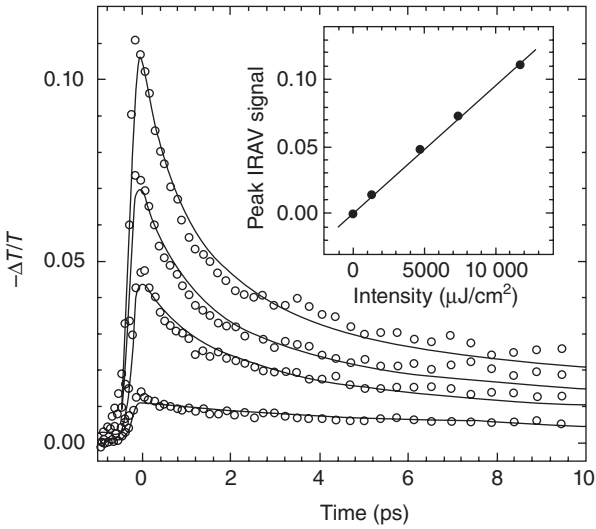

11.5 Intensity dependence of the transient IRAV signal in oriented PPV, measured with perpendicular pump polarization and parallel probe polarization with respect to the polymer chain axis. Reprinted with permission from Soci, C., Moses, D., Xu, Q. H. & Heeger, A. J. 2005. Charge-carrier relaxation dynamics in highly ordered poly(*p*-phenylene vinylene): Effects of carrier bimolecular recombination and trapping. *Physical Review B*, **72**. Copyright (2005) by the American Physical Society (DOI: 10.1103/PhysRevB.72.245204).

by photocarrier generation, a short circuit between two ends of a gap in a microstrip waveguide, as shown in Fig. 11.6(a). A short wavelength 'on' pulse absorbed near the surface of the silicon substrate is used for photoexcitation. A consecutive 'off' pulse with higher wavelength and hence higher penetration depth creates a short circuit between the ground plane and the waveguide. With this configuration, pulses with a length controlled by the delay between on and off pulses can be generated. If only the 'on' pulse was used, the length of the generated electrical pulse would be determined by the carrier lifetime of the silicon substrate. However, the delay between 'on' and 'off' pulses can be controlled on a timescale orders of magnitude smaller.

The same device can be used for pulse generation, by applying a DC bias on the input, or for optical sampling of an incoming arbitrary waveform. Evolutions of the device consisted in replacing the silicon substrate with other materials having shorter-lived carrier lifetimes, to eliminate the need for the off pulse. Instead of shining the off pulse, cross-correlation of the generated electrical pulse can be obtained by a sampling probe pulse (Fig. 11.6(b)). Radiation damaged or implanted materials (Smith *et al.*, 1981; Ketchen *et al.*, 1986), amorphous materials (Auston *et al.*, 1980) and advanced

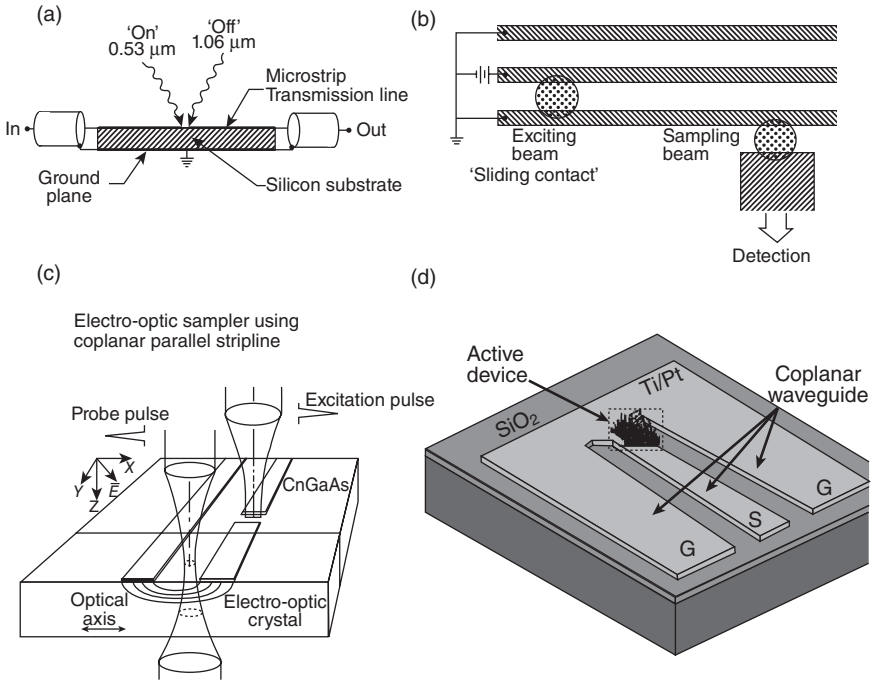

11.6 (a) An optoelectronic gate switches on by absorption of 0.53 μm pulse and switches off by a delayed 1.06 μm pulse. (b) Coplanar transmission line consisting of three parallel 5 μm wide Al lines separated by 10 μm. Also shown is the 25 μm wide sampling probe separated by a 10 μm gap from the transmission line. The exciting and sampling laser beams are indicated by the circles. The DC bias was 20 V. (c) Electro-optic sampler arrangement with coplanar strip geometry. (d) Illustration of the InP-nanowire high-speed photoconductor. Reprinted with permission from: (a) Auston, D. H. 1975. Picosecond optoelectronic switching and gating in silicon. *Applied Physics Letters*, **26**, 101–103, Copyright (1975), American Institute of Physics (DOI: 10.1063/1.88079.); (b) Ketchen, M. B., Grischkowsky, D., Chen, T. C., Chi, C. C., Duling, I. N., Halas, N. J., Halbout, J. M., Kash, J. A. & Li, G. P. 1986. Generation of subpicosecond electrical pulses on coplanar transmission-lines. *Applied Physics Letters*, **48**, 751–753, Copyright (1986), American Institute of Physics (DOI: 10.1063/1.96709); (c) Mourou, G. A. & Meyer, K. E. 1984. Subpicosecond electro-optic sampling using coplanar strip transmission-lines. *Applied Physics Letters*, **45**, 492–494, Copyright (1984), American Institute of Physics (DOI: 10.1063/1.95312); (d) Logeeswaran, V. J., Sarkar, A., Islam, M. S., Kobayashi, N. P., Straznicky, J., Li, X., Wu, W., Mathai, S., Tan, M. R. T., Wang, S.-Y. & Williams, R. S. 2008. A 14-ps full width at half maximum high-speed photoconductor fabricated with intersecting inp nanowires on an amorphous surface. *Applied Physics A: Materials Science & Processing*, **91**, 1–5. Copyright (2008), with permission from Springer (DOI: 10.1007/s00339-007-4394-x).

MBE grown composite materials such as low-temperature grown GaAs (Smith *et al.*, 1989) were used for the switch.

Although the same photoconductive switch is suitable for both photocurrent generation and sampling, later research focused on sampling the propagating pulse by electro-optic effects, which enabled all-optical detection. Pockels cells were first built on $LiNbO_3$ crystals (Valdmanis *et al.*, 1982); $LiTaO_3$ was later used as optoelectric material (Valdmanis *et al.*, 1983). Furthermore, the performance is increased by switching to thinner substrates (Holzman *et al.*, 2000) or to coplanar transmission line design (Fig. 11.6(c)) (Mourou and Meyer, 1984) since in microstrip design, the line spacing is governed by substrate thickness and dispersion becomes important at frequencies where the wavelength drops below the line spacing. A major progress was the sampling of the pulse by exploiting the Franz–Keldysh effect (Lampin *et al.*, 2001) which is a particularly sensitive optoelectric effect and offers the advantage that the device including emitter and detector can be fabricated monolithically on SI GaAs substrate carrying a LT-GaAs epilayer.

Auston switches are used for generating few-oscillation pulses that can be used for transmission line spectroscopy or transformed into free-space radiation in combination with antennas. An application with particular importance for organic electronics is an Auston switch implemented by depositing a transmission line gap over an organic semiconductor with unknown optoelectric properties. This method is often referred to as TPC spectroscopy and will be described in detail in the next section. The photoconductive switch is mostly implemented as microstrip design since organic semiconductors are often incompatible with the use of standard photolithographic methods because of the need of chemical resists. Examples of coplanar design do, however, exist (Logeeswaran *et al.*, 2008) and yield performance gains of an order of magnitude. Their schematic is shown in Fig. 11.6(d).

In recent work, we applied electromagnetic modeling to Auston switch structures (Diesinger *et al.*, 2011, 2012) with two main objectives:

1. Assessing the potential of a switch structure featuring a transition from microstrip gap to coplanar accesses: with this approach, a gap can be defined on organic semiconductors by compatible deposition techniques and the performance of coplanar design could still be approached by optimization of the transition.
2. Decomposing the Auston switch into a hybrid model, consisting of intrinsic material response and structural response. The signal deterioration due to the structural response can then be eliminated by deconvolution, yielding the intrinsic material response with the fastest achievable time resolution.

The photoconductive switch was modeled as a 4-port S-matrix (see Fig. 11.7). The S-parameters were calculated by the electromagnetic modeling tool High Frequency Structure Simulator (HFSS) and used to describe the structural response of the switch as transimpedance function between the current generated in the unknown material and the output signal propagating along the transmission line. Previous approaches based on a description of the switch by S-parameters (Green and Sobolewski, 2000; Tripon-Canseliet *et al.*, 2006) were fundamentally different since they aimed at computing the transfer between input and output ports rather than representing the active area by a current generator and describing the effect of the structure as a transimpedance.

11.3.2 Acquisition of photocurrent transients

The TPC characterization method consists of incorporating an unknown semiconductor into an Auston switch that is DC biased on one side, and in observing, on a fast oscilloscope or boxcar integrator, a photocurrent transient generated in response to a negligibly short laser pulse incident on the switch. A summary of application of the method on molecular crystal, polymers, polymer blend is given in following paragraphs.

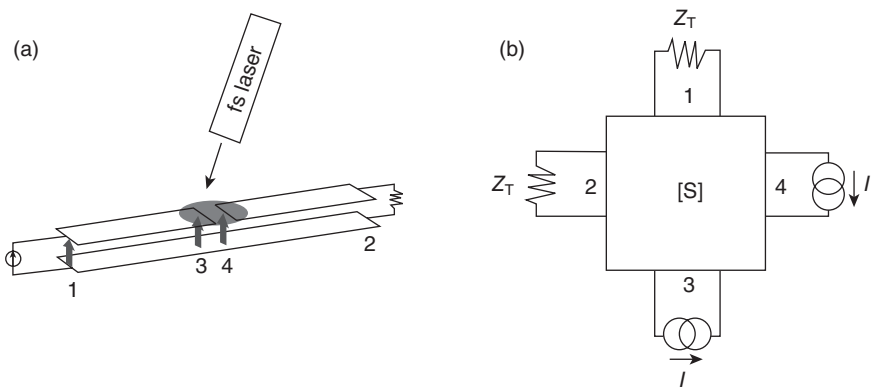

11.7 Approach of modeling a photoconducive gap in a microstrip as 4-port S-matrix: (a) schematic of the microstrip gap with active material (oval spot) with port assignment; (b) equivalent circuit; outer ports 1 and 2 are considered to be terminated with the transmission line impedance Z_T, while inner ports 3 and 4, located at the transmission line edges, are open. Adapted from Diesinger, H., Panahandeh-Fard, M., Baillargeat, D. & Soci, C. 2011. Electromagnetic modeling and optimization of photoconductive switches for terahertz generation and photocurrent transient spectroscopy. *Proceedings of the 2011 IEEE MWP*, 373–376 (DOI: 10.1109/MWP.2011.6088749).

Molecular crystals

Models for the carrier photoexcitation mechanism in molecular crystals have been established initially on the bases of measurements on oligoacenes and later applied to conjugated polymers as well. These models (e.g. the Onsager model) emphasize the localized nature of photoexcitations and describe carrier generation as a secondary process involving exciton dissociation. Moses *et al.* (2006) showed that for crystalline tetracene, the predictions of the Onsager model are at variance with experimental data. The peak height of photocurrent transients increased for lower temperatures, in contrast to the DC photocurrent. By normalizing PC transients to a constant peak height, it was shown that the T dependence of the tail was opposite to the peak T dependence, revealing two transport mechanisms corresponding to an initial peak due to carriers occupying extended states and a slower decay corresponding to thermally activated hopping. This is shown in Figs 11.8 and 11.9. A study on functionalized pentacene, comparing optical pump THz probe and PC transient, has been presented by Hegmann *et al.* (2004). The conclusions are similar to the case of tetracene, where the height of the initial peak that rises within 0.5 ps (limited by the resolution of the THz probe) increases with decreasing temperature.

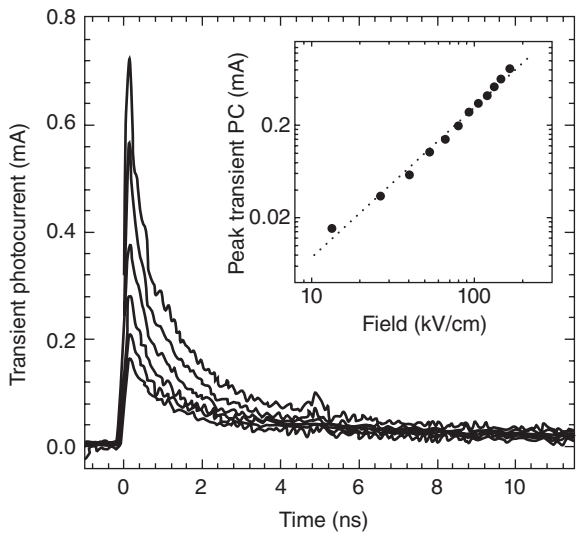

11.8 Photocurrent transients measured at different temperatures, *T* increasing from top to bottom; the inset shows the field dependence of the peak height. Reprinted with permission from Moses, D., Soci, C., Chi, X. L. & Ramirez, A. P. 2006. Mechanism of carrier photogeneration and carrier transport in molecular crystal tetracene. *Physical Review Letters*, **97**, 067401. Copyright (2006) by the American Physical Society (DOI: 10.1103/PhysRevLett.97.067401).

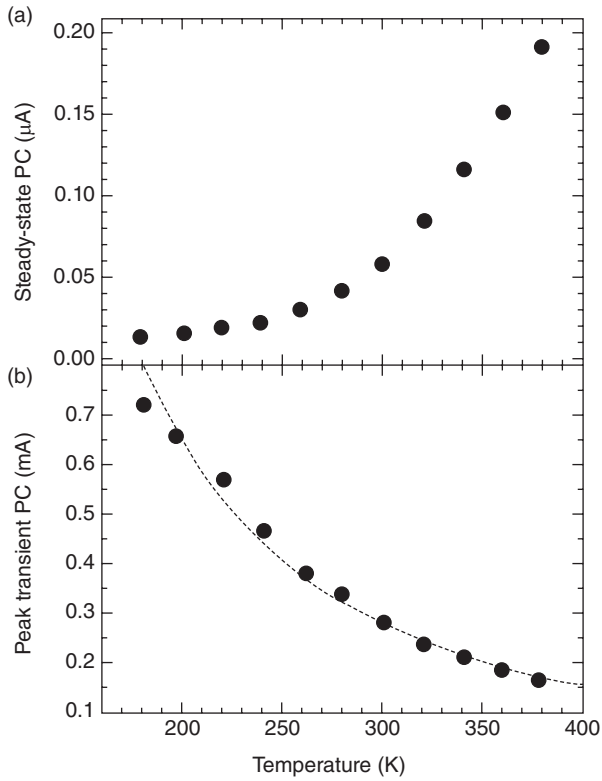

11.9 Temperature dependence of steady state PC vs temperature dependence of the transient peak height. Reprinted with permission from Moses, D., Soci, C., Chi, X. L. & Ramirez, A. P. 2006. Mechanism of carrier photogeneration and carrier transport in molecular crystal tetracene. *Physical Review Letters*, **97**, 067401. Copyright (2006) by the American Physical Society (DOI: 10.1103/PhysRevLett.97.067401).

Polymers

Moses, Sinclair, and Heeger first used transient photocurrent spectroscopy to study the photogeneration and transport properties of polydiacetylene-(bis *p*-toluene sulfonate) (PDA-TS), showing that the carrier generation is in disagreement with the Onsager model (Moses *et al.*, 1987). Temperature and field-dependent transients showed a temperature-independent initial peak due to hot carriers and a thermally activated tail attributed to trap dominated transport. The temperature and field independence of initial generation quantum yield shows that the Onsager model is also not applicable in this organic polymer crystals. The time resolution of the measurement was 3 ns and the transient, including the tail, around 30 ns.

A study by Moses *et al.* (2006) on PPV and its derivatives using a combination of IRAV PIA spectroscopy and photocurrent transient spectroscopy shows that polarons and excitons are both independent primary excitations. An apparent increase of photoconductivity at photon energies above 3–4 eV is due to external currents induced by electron photoemission, an experimental artifact. Using a quenching gas to suppress photoemitted electrons, the photoconductivity becomes nearly independent on photon energy.

Soci *et al.* (2005) studied charge carrier dynamics in highly ordered PPV by IRAV PIA and photoconductance transient on a 10 ps and 20 ns timescale respectively. At short times after the photoexcitation (10 ps, as measured by IRAV), the carrier dynamics follows a decay largely dominated by bimolecular recombination, as shown in Fig. 11.10. At longer times (20 ns, as obtained by TPC measurements), the carrier dynamics is the result of a system of differential equations that include bimolecular recombination

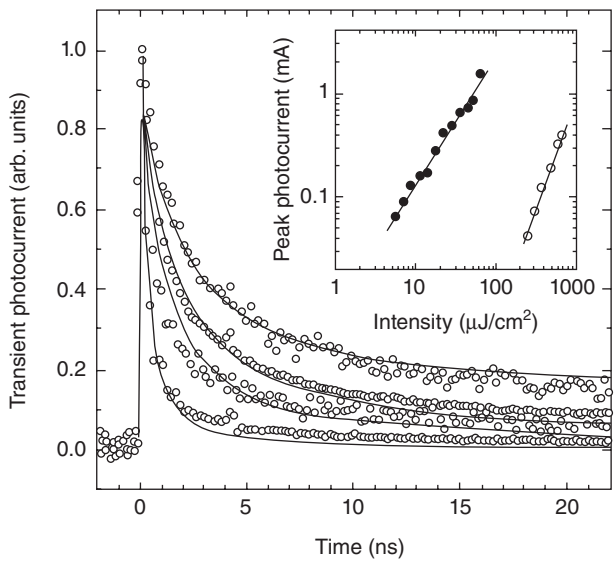

11.10 Photocurrent transient of highly ordered PPV sample for different intensities increasing from top to bottom, normalized at $t = 0$; the solid lines are the solutions of the carrier dynamic differential equation; the inset shows the peak height as function of excitation intensity for one- and two-photon excitation (solid and open circles respectively). Reprinted with permission from Soci, C., Moses, D., Xu, Q. H. & Heeger, A. J. 2005. Charge-carrier relaxation dynamics in highly ordered poly(*p*-phenylene vinylene): Effects of carrier bimolecular recombination and trapping. *Physical Review B*, **72**, 245204. Copyright (2005) by the American Physical Society (DOI: 10.1103/PhysRevB.72.245204).

(with the same coefficient as determined for first 10 ps), trapping, detrapping, and recombination of trapped carriers with free carriers of opposite sign. It is noteworthy that monomolecular recombination is not needed to describe the carrier dynamics. It is suggested that in other conjugated polymers where the free carrier density is described by an initial fast exponential decay followed by a slower stretched exponential, the mechanism responsible of the fast exponential is trapping rather than monomolecular recombination. Due to the highly ordered material used in this study, the initial decay is dominated by bimolecular recombination and the trapping becomes important at timescales observed by TPC. The time resolution of IRAV and PC transient were 300 fs and 100 ps, respectively, and the observation intervals of the above examples were 10 ps for IRAV and 20 ns for PC transient.

Polymer blends

Soci *et al.* (2007) compared photoresponsivities and photocurrent transients of pristine polymers P3HT and poly[2,6-(4,4-bis-(2-ethylhexyl)-4H-cyclopenta[2,1-b;3,4-b′]dithiophene)-alt-4,7-(2,1,3-benzothiadiazole)] (PCPDTBT) with corresponding bulk heterojunction blends of these polymers with a fullerene derivative (phenyl-C61-butyric acid methyl ester, PCBM). They found a 100-fold increase in DC photoresponsivities and the appearance of a photocurrent tail that decays within few nanoseconds, whereas the prisitine polymers show a TPC peak of less than 100 ps wide and limited by instrumental resolution. The identical effect of the blend on PCPDTBT as on P3HT, in combination with the lower bandgap of PCPDTBT, makes this polymer promising for high energy conversion efficiency solar cells.

Timescales

The time resolution of the technique is currently about 100 ps. The limitation is essentially due to the structural response of an Auston switch implemented as gap in a microstrip line, as discussed by Diesinger *et al.* (2012). By optimizing the switch design and deconvolving its response from the experimental transient, a resolution of 10 ps and less can be achieved. The time interval of the observation is limited only by the memory and sampling interval of the storage oscilloscope typically used.

11.4 Time-resolved terahertz spectroscopy (TRTS)

Time-resolved terahertz (THz) spectroscopy of organic semiconductors typically employs an optical pump pulse and a THz probe which is

non-resonant with the bandgap to monitor the charge carriers generated upon photoexcitation. As in conventional pump-probe techniques, the relative change in transmission of the THz pulse induced by the pump beam, $\Delta T/T_0$, is monitored as a function of the delay time of the THz probe with respect to the pump pulse. Next, the change in transmission coefficient is related to the refractive index or, via Fresnel-like equations, to the conductivity change of the sample. Often, it is found that the response of the sample is independent of frequency in the spectral range of the THz pulse, hence the differential transmission is directly related to the DC conductivity. In the simplest case (Hegmann *et al.*, 2002), a linear relation between the relative differential transmission and the DC conductivity is assumed (Fig. 11.11). We will now mention applications of this technique to the study of charged photoexcitations in organic semiconductors; for a general review on Terahertz spectroscopy applied to the study of carrier dynamics in semiconductors we refer the reader to Ulbricht *et al.* (2011).

11.4.1 Molecular crystals

Optical-pump THz-probe spectroscopy was performed on a number of molecular crystals, including pentacene, rubrene, tetracene and pentacene bulk crystals (Thorsmolle *et al.*, 2004; Ostroverkhova *et al.*, 2005a, 2006) and their films (Ostroverkhova *et al.*, 2005b).

Hegmann *et al.* (2002) suggest that in functionalized pentacene, mobile carriers are a primary photoexcitation because of the subpicosecond rise-time of the photoconductivity. Furthermore, it was found that the measured photoconductance is independent on the amplitude of the THz field peak in contradiction with field induced exciton dissociation; the generation of mobile carriers in less than 0.5 ps, i.e. below the system resolution, is in agreement with previous studies by Miranda *et al.* (2001) and Moses *et al.* (2000). At times $t > 4$ ps, the photoconductivity decay was found to follow a $t^{-\beta}$ law, indicative of dispersive transport. The exponent beta was found to be nearly temperature independent between 10 and 300 K. This is inconsistent with multiple trapping models. Temperature dependence does exist for the amplitude of the initial peak that increases with decreasing temperature, indicative of bandlike transport. The time resolution of the photoconductivity measurement is limited by the THz probe pulse to some picoseconds, and the observation interval here is about 40 ps due to the fast decay time. The observation interval could be made longer by using longer delay stages (e.g. a mechanical delay of 30 cm would correspond to a nanosecond optical delay). Thorsmolle *et al.* (2004) found similar results in pentacene and provide an estimate for the carrier mobility based on the number of absorbed photons and the observed conductivity peak.

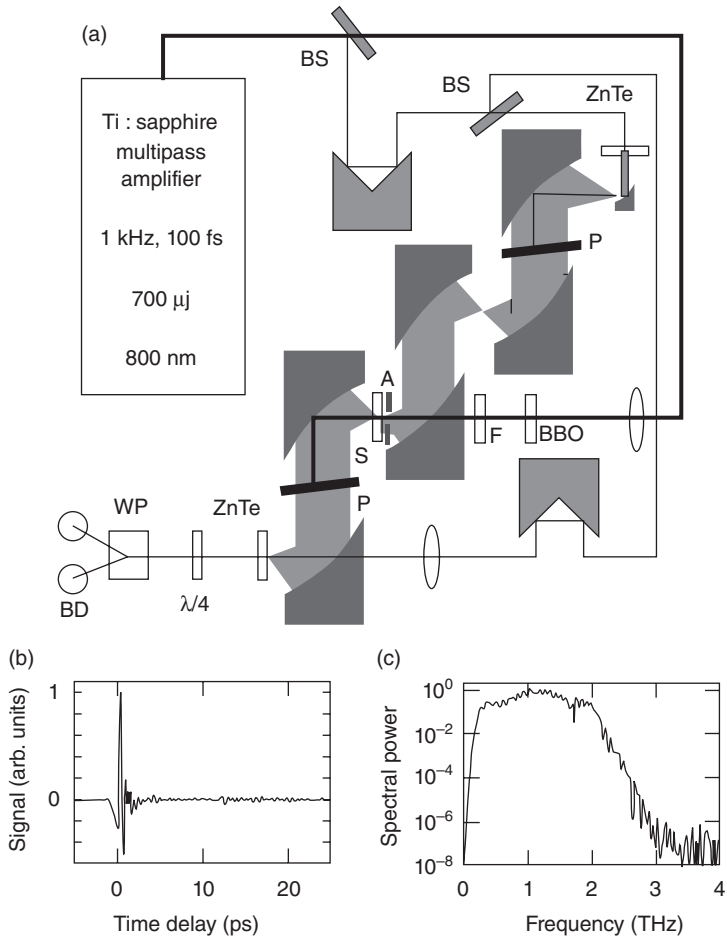

11.11 (a) Schematic of the THz apparatus. BS: beam splitter; P: polyethylene visible beam block; F: blue filter; S: sample; A: 1 mm aperture; l/4: quarter-wave plate; WP: Wollaston prism; and BD: balanced detector. Gold coated parabolic mirrors are used to direct the THz pulse through the system. (b) Single-scan THz trace; full width at half maximum 250 fs and (c) spectrum obtained under dry N_2. The oscillatory nature of the spectrum is an artifact resulting from multiple reflections of the THz pulse. Reprinted with permission from Lui, K. P. H. & Hegmann, F. A. 2001. Ultrafast carrier relaxation in radiation-damaged silicon on sapphire studied by optical-pump-terahertz-probe experiments. *Applied Physics Letters*, **78**, 3478–3480, Copyright (2001), American Institute of Physics (DOI: 10.1063/1.1375841).

Carrier mobility in pentacene was again observed to increase from room temperature down to 30 K, indicative of bandlike transport. It was also found that the initially free carriers became trapped within few picoseconds.

The study by Ostroverkhova *et al.* (2005a) on crystals of a pentacene derivative functionalized with triisopropylsilylethynyl (TIPS) side groups and pentacene thin films confirmed initial bandlike transport by the temperature dependence of the initial peak. It is emphasized that bandlike mobility increases with temperature, where temperature activated mobility had not been previously reported in polyacene thin films. In thin films, the photoconductivity decay is described by a single exponential. In contrast to the single crystal where the photoconductivity follows a $t^{-\beta}$ behavior, the single exponential decay is attributed to fast carrier capture by deep traps at the grain boundaries. Ostroverkhova *et al.* (2006) compared the carrier dynamics of pentacene, functionalized pentacene, tetracene, and rubrene single crystals. Fast charge carrier photogeneration and bandlike charge transport were confirmed for all these samples. The decay dynamics were studied as function of temperature down to 20 K. A transition to faster decay dynamics in pentacene single crystals was observed below 70 K. At low temperature, the power law exponent of functionalized pentacene was found to be temperature independent, while in pentacene the exponent beta went from 0.6 to 1.2 for temperatures from 100 K down to 5 K. These findings suggest that in pentacene carriers are trapped by shallow traps at very low temperature, whereas such traps are absent in functionalized pentacene.

Ostroverkhova *et al.* (2005b) then studied pentacene and functionalized pentacene thin films with respect to their fabrication methods. One of the films of functionalized pentacene evaporated at 25 °C, exhibiting the fastest decay dynamics described by a single-exponential $e^{t/\tau}$ with $\tau = 0.6$ to 1.4 ps. In contrast, in films evaporated at 85 °C and in solution grown functionalized pentacene, the decay could be fitted by the power-law function $t^{-\beta}$ with $\beta = 0.53$ over at least 100 ps, as shown in Fig. 11.12. The different decay dynamics are attributed to the structure: functionalized pentacene evaporated at 25 °C shows small interconnected domains in atomic force microscpy (AFM) images. The fast single exponential decay is attributed to fast trapping on grain boundaries, whereas the larger crystallites obtained by evaporation at 85 °C and solution grown films lead to longer carrier lifetimes and power law decays similar to single crystal over more than 100 ps. Pristine pentacene samples showed a decay that could be fitted by a biexponential function. The deep-level trapping on grain boundaries, defects, and/or chemical impurities prevented the observation of the carrier transport on time scales above 20–30 ps after photoexcitation.

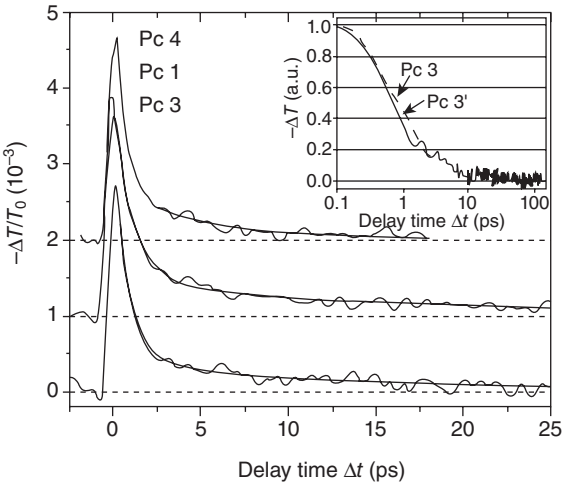

11.12 Differential transmission $-\Delta T/T_0$ as a function of pump-probe delay time Δt obtained in Pc 1 (evaporated on KCl at 35 °C), Pc3 (evaporated on mica at 35 °C), and Pc4 (evaporated on glass at 25 °C) thin films under optical excitation at 580 nm in air at room temperature. Fits with a biexponential function are also shown. The inset shows the ΔT transients normalized to their values at Δt=0 obtained under the same conditions in the Pc 3 and Pc 3′ films. Reprinted with permission from Ostroverkhova, O., Shcherbyna, S., Cooke, D. G., Egerton, R. F., Hegmann, F. A., Tykwinski, R. R., Parkin, S. R. & Anthony, J. E. 2005. Optical and transient photoconductive properties of pentacene and functionalized pentacene thin films: Dependence on film morphology. *Journal of Applied Physics*, **98**, 033701. Copyright (2005), American Institute of Physics (DOI: 10.1063/1.1949711).

11.4.2 Polymers

In contrast to the above cases where the response of the investigated film to the photoexcitation is a purely real conductivity, examples exist in the literature where a phase shift of the transmitted THz pulse and hence complex conductivity has been observed. For instance, the transient photoconductivity of GaAs (bulk and nanowires) (Beard *et al.*, 2000; Parkinson *et al.*, 2007) has been interpreted in terms of Drude-like charge carrier dynamics.

The method has been applied by Hendry *et al.* (2006) to the polymers MEH-PPV and rr-P3HT. It was found that in rr-P3HT, the complex conductivity has real and imaginary components that both increase with frequency between 0.3 and 1.3 THz, and decay similarly on the observation timescale of some nanoseconds. MEH-PPV has a frequency-dependent real conductivity that decays within some picoseconds and a

frequency-dependent imaginary component that decays over some hundreds of picoseconds. The behavior of rr-P3HT is interpreted by a model based on tight binding approximation and attributed to free charges. The purely imaginary (long-term) conductivity component of MEH-PPV has been attributed to exciton polarizability. Here the time resolution was 3 ps, similar to the previous case of molecular crystals; due to the relatively slow decay of the photoinduced free and localized charges in these partially ordered polymers, the observation interval in this example was 10 ns.

Unuma *et al.* (2010) used THz spectroscopy to measure the complex conductivity of doped polythiophenes (P3HT and PEDOT) without optical pumping by interpreting their data within the Drude–Smith model. They concluded that carriers are partly localized and that the degree of localization depends on carrier density. Here, time resolution and observation interval are not applicable because the carriers in the sample are induced by static doping.

11.4.3 Polymer donor–acceptor blends

Cunningham and Hayden (2008) performed optical pump Thz probe measurements on P3HT and a P3HT:PCBM blends and modeled the carrier dynamics by the Drude–Smith model. They found that the blend has a higher photocarrier generation yield but a lower mobility than the pristine P3HT. Observation interval is up to 100 ps and time resolution is claimed to be subpicosecond.

Nemec *et al.* (2009) studied a low band-gap polyphenylene copolymer (LBPP-1) blended with PCBM for which the complex conductivity is measured by optical-pump THz-probe spectroscopy. Here the analysis was not based on the assumption that the decay of the photoconductance is small during the THz probing interval; instead, the data were analyzed in 2D frequency space, in which one frequency represents the spectrum of the decay and the other the spectrum of the probe pulse. The complex conductivity was compared to the response predicted by Monte-Carlo simulations rather than from the Drude–Smith model which, according to the authors, is a purely phenomenological description. Time resolution was again on the order of 2.3 ps, and the pump probe delay was swept from 2.5 to 50 ps.

11.5 Time-resolved microwave conductivity (TRMC)

TRMC is a contactless conductivity probing technique that consists in measuring the transmission of a microwave signal across the sample as a function of delay between a pump pulse (visible laser in flash-photolysis TRMC or gamma radiation in the MeV range in pulse-radiolysis TRMC) and the microwave probe pulse. A polymer-coated quartz plate is placed in

a microwave resonant cavity at a position of maximum electric field strength, as shown in Fig. 11.13. The photoinduced change in the conductance of the sample upon flash photolysis, ΔG, is monitored as a change in the microwave power, $\Delta P/P$, reflected by the cavity at resonance using microwave circuitry and detection equipment. As microwave source, a Gunn oscillator operating at about 9 GHz and with an output power of about 100 mW is typically used. Microwaves reflected by the cell are detected by a Schottky barrier diode detector. The change in reflected microwave power is in the simplest case and within certain limits proportional to the change in conductance of the polymer film. The response time of such cavities is typically around 40 ns, due to the Q-factor of the resonance. The excitation can hence be performed by a ns laser rather than a fs laser. In contrast to optical pump terahertz probe with ps resolution, the microwave signal is CW at 9 GHz, so observation of microwave reflectance is performed electrically by a detection circuitry and an oscilloscope rather than by optical delay stages, and the interval of observation is typically over hundreds of nanoseconds, out of the typical range of delay stages. Application of this somewhat slower technique is to the observation of charges generated in polymers; the lifetime of the singlet exciton is shorter than the excitation pulse (hence steady state of singlet excitons establishes during the excitation), but the free charges, whether dissociated excitons or directly generated, do have lifetimes in the range of this long timescale.

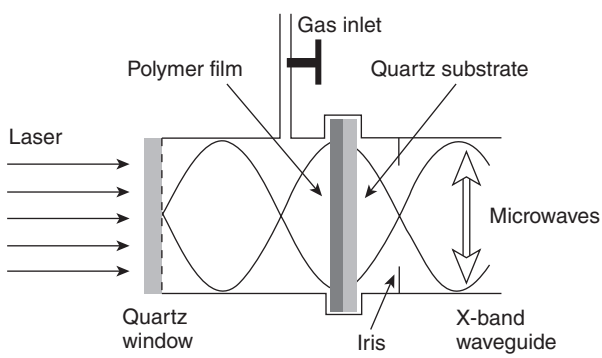

11.13 Schematic representation of the microwave resonant cavity containing a thin-layer sample (not to scale). The sinusoidally varying dashed lines represent the standing-wave pattern of the microwave electric field. Reprinted with permission from Dicker, G., De Haas, M. P., Siebbeles, L. D. A. & Warman, J. M. 2004. Electrodeless time-resolved microwave conductivity study of charge-carrier photogeneration in regioregular poly(3-hexylthiophene) thin films. *Physical Review B*, **70**, 045203. Copyright (2004) by the American Physical Society (DOI:10.1103/PhysRevB.70.045203).

Historically, TRMC was developed for detection of transient ionic conductivity of pulse irradiated dielectric liquids (Infelta *et al.*, 1977) and derived from pulse radiolysis with optical detection. Later, the evolution from pulse radiolysis to flash photolysis (De Haas and Warman, 1982) consisted of extending the detection from charge separation induced by high energetic 'ionizing' pulses to photon absorption-induced charge separation. Even before this, the sensitivity and time resolution was increased to enable studying the geminate decay of molecular ions in liquids (Bao *et al.*, 1996; Sirringhaus *et al.*, 1998; Brown *et al.*, 2001). In the case of polymer films, the photoinduced conductance of the sample proportionally reduces the microwave power reflected from the microwave chamber. The conductance is then plotted as function of time, which typically yields a multiexponential decay. The temporal decay function is not always analyzed.

11.5.1 Molecular crystals

Saeki *et al.* (2006) measured the photoinduced transient conductivity of pentacene by TRMC. The real and imaginary components of the conductivity were separated. As excitation source, an ArF excimer laser, 193 nm wavelength, with 35–30 ns FWHM was used. The conductivity values were compared to molecular orbital calculations. The decay constant was found to be much faster than expected triplet lifetime. An explanation is that triplets might be quenched by interaction with oxygen and that a high incident photon density may promote triplet–triplet annihilation. The observation interval was limited here to 2 μs due to the fast decay. It can be made as long as desired by choosing the range on the oscilloscope.

11.5.2 Polymers

Dicker *et al.* (2004) found that the conductance change of a regioregular P3HT film is proportional to the absorbed photons at the onset of the curve and proportional to the square root of it above a critical value (Fig. 11.14). This behavior was attributed to the transition from monomolecular to bimolecular recombination, either of the excitons (exciton annihilation) or charge carrier bimolecular recombination. Furthermore, it is related to the lamellar character of the regioregular P3HT: below the threshold of one excited state per lamellae, the recombination is monomolecular. This is in agreement with other works that attribute the reduced bimolecular recombination rate to the two-dimensional character of the conduction (Sirringhaus *et al.*, 1999; Osterbacka *et al.*, 2000; Brown *et al.*, 2001; Juška *et al.*, 2009; Osterbacka *et al.*, 2010). The decay of the photoinduced conductivity was shown over some hundred nanoseconds. The decay waveform, however, was not analyzed in detail.

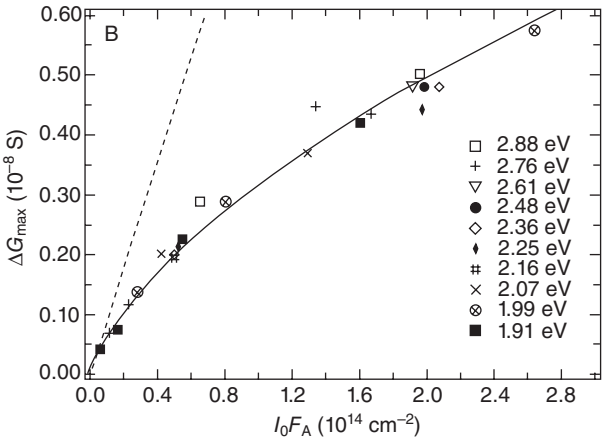

11.14 The dependence of the maximum photoconductance, ΔG_{max}, for a 110 nm film on the product of the incident intensity, I_0, and the fraction of photons absorbed in the sample, *FA*, for photon energies below 3 eV. The data for I_0F_A values are expanded. The full line was calculated and the dashed straight line corresponds to the limiting, low-intensity linear dependence. Reprinted with permission from Dicker, G., De Haas, M. P., Siebbeles, L. D. A. & Warman, J. M. 2004. Electrodeless time-resolved microwave conductivity study of charge-carrier photogeneration in regioregular poly(3-hexylthiophene) thin films. *Physical Review B*, **70**, 045203. Copyright (2004) by the American Physical Society (DOI: 10.1103/PhysRevB.70.045203).

11.5.3 Polymer donor–acceptor blends

The method has also been applied to blends of P3HT:PCBM and pDA2T:PCBM, showing that, upon thermal annealing, the photocarrier generation yield is reduced but the carrier lifetime increases, which is overall beneficial for the photoconversion efficiency of solar cells (Grzegorczyk *et al.*, 2008). Decay times for the pDA2T blend are on the order of microseconds.

Savenije *et al.* (2011) found that, in blends of P3HT:PCBM, charges do not undergo post-nanosecond relaxation into deep traps. By temperature-dependent TRMC, they determined activation energies of 10 meV and 80 meV attributed to hole and electron transport.

Rance *et al.* (2011) studied blends of the polymer poly(2,5-bis(3-tetradecylthiophen-2-yl)thieno[3,2-b]thiophene) (pBTTT) with $PC_{71}BM$ and bis-$PC_{61}BM$, for which the high-frequency carrier mobility is determined from the peak conductance of the TRMC. It is found that the pBTTT:$PC_{71}BM$ blend shows enhanced electron mobility as a result of its intercalated structure with pure PCBM domains, while the pBTTT:bis-$PC_{61}BM$ blend shows

hole-dominated conductance with carrier mobility independent of bi-PCBM loading, due to the non-intercalated structure.

11.6 Experimental evidence of charge localization

In the field of organic photovoltaics, a major issue which affects power conversion efficiency is the localization of charges at different scales. Initially, excitons and free charges in band-like states are photogenerated simultaneously. Some excitons dissociate, while extended band-like states thermalize, take part in dispersive transport, or become trapped in more or less shallow traps, giving rise to thermally activated transport. While PIA spectroscopy cannot distinguish directly between polarons and excitons (if not coupled to magnetic spin measurements), photocurrent measurements have the opposite limitation of detecting exclusively charge carriers that are free on the entire device scale. In the following, it shall be discussed to which extent the three methods of TRTS, TRMC and TPC described previously for the characterization of prompt (sub-nanosecond) transport properties are appropriate for detecting partially located charges.

The response of a material containing free and localized charges can be described by a simple expression. The conductivity due to the free carriers is often described by the Drude model containing a force to overcome the inertial moment of the carriers and a viscous drag force:

$$\sigma_f(\omega) = \frac{N_f e^2 \tau_f}{m(1 - i\omega\tau_f)} \qquad [11.1]$$

where N_f is the carrier density, e the elementary charge, τ_f the momentum relaxation time, and m the carrier mass. If $\omega << 1/\tau_f$, the response of the material to an external electric field is described by a purely real conductivity:

$$\sigma_f = \frac{N_f e^2 \tau_f}{m} \qquad [11.2]$$

The localized charges contribute a permittivity that is described by several, or in the most primitive case a single, oscillator strength:

$$\epsilon_l(\omega) = \frac{N_l e^2}{m(\omega_0^2 - \omega^2)} \qquad [11.3]$$

where ω_0 is the resonance frequency. For simplicity the expression contains no dissipative term.

When the response of the photoexcited material is measured in terms of a 'complex conductivity', the contribution from localized charges is reflected by an imaginary term $i\omega\varepsilon_l$, and the entire conductivity writes:

$$\sigma = \sigma' + i\sigma'' = \frac{N_f e^2 \tau_f}{m} + i\omega \frac{N_l e^2}{m(\omega_0^2 - \omega)} = \sigma_f + i\omega\varepsilon_l \qquad [11.4]$$

This corresponds to the description of a lossy dielectric medium and predicts a frequency-independent real part and a frequency-dependent imaginary part of the complex conductivity. Stronger carrier localization translates into a higher ω_0, and the higher the probing frequency ω needs to be to make the imaginary conductance discernible. In the literature, the Drude–Smith model, an extension of the Drude model with the objective of taking into account partly localized carriers, is more frequently seen than the above oscillator model (Smith, 2001). It has been used in THz probe spectroscopy (Unuma *et al.*, 2010) and optical-pump THz-probe spectroscopy (Cunningham and Hayden, 2008). The Drude–Smith model also predicts a rise of the real part of the conductance with increasing frequency. An alternative approach is given by the interpretation of experimental data in terms of the Kubo formalism (Prins *et al.*, 2006).

We illustrate the measurement of photoinduced complex conductivity with examples from the literature: Hendry *et al.* (2006) have studied the complex photoconductivity of rr-P3HT films and MEH-PPV films by TRTS and observed that the THz pulse transmitted through the photoexcited material is subject to a phase shift (Fig. 11.15(a)). Spectra for the real and imaginary parts of the conductivities are derived by Fourier analysis and repeated for different pump-probe delay times. Both real and imaginary components increase for increasing frequency throughout the spectrum in the range from 0.3 to 1.3 THz (Fig. 11.15(c) and (e)). For P3HT real and imaginary components at the probing frequency of 0.6 THz are of the same order of magnitude throughout the observation time interval (Fig. 11.15(b–d)), while for MEH-PPV the real part of the conductivity decays within picoseconds and afterwards the conductivity is almost purely imaginary (Fig. 11.15(e, f)). This difference is explained by the presence of long-lived mobile carriers in P3HT, whereas in MEH-PPV carriers decay within few picoseconds and the purely imaginary part is ascribed to exciton polarizability.

In the case of TRMC, the complex conductivity was measured in pentacene by Saeki *et al.* (2006). The complex conductivity of the film obtained after determining the evolution of the Q-factor of the resonance chamber (by fitting a resonance curve over a Gunn diode frequency interval that changes around 9 GHz, with a relative change of 10^{-5}) is shown in Fig. 11.16. In this case the imaginary component of the conductivity is small compared to the real part; Moreover, these data do not allow verifying the frequency dependence of the imaginary part of the conductivity (as predicted by Eq. 11.5) over a wide range due to the very narrow frequency range imposed by the fitting procedure. In contrast, the center frequency of a THz burst is

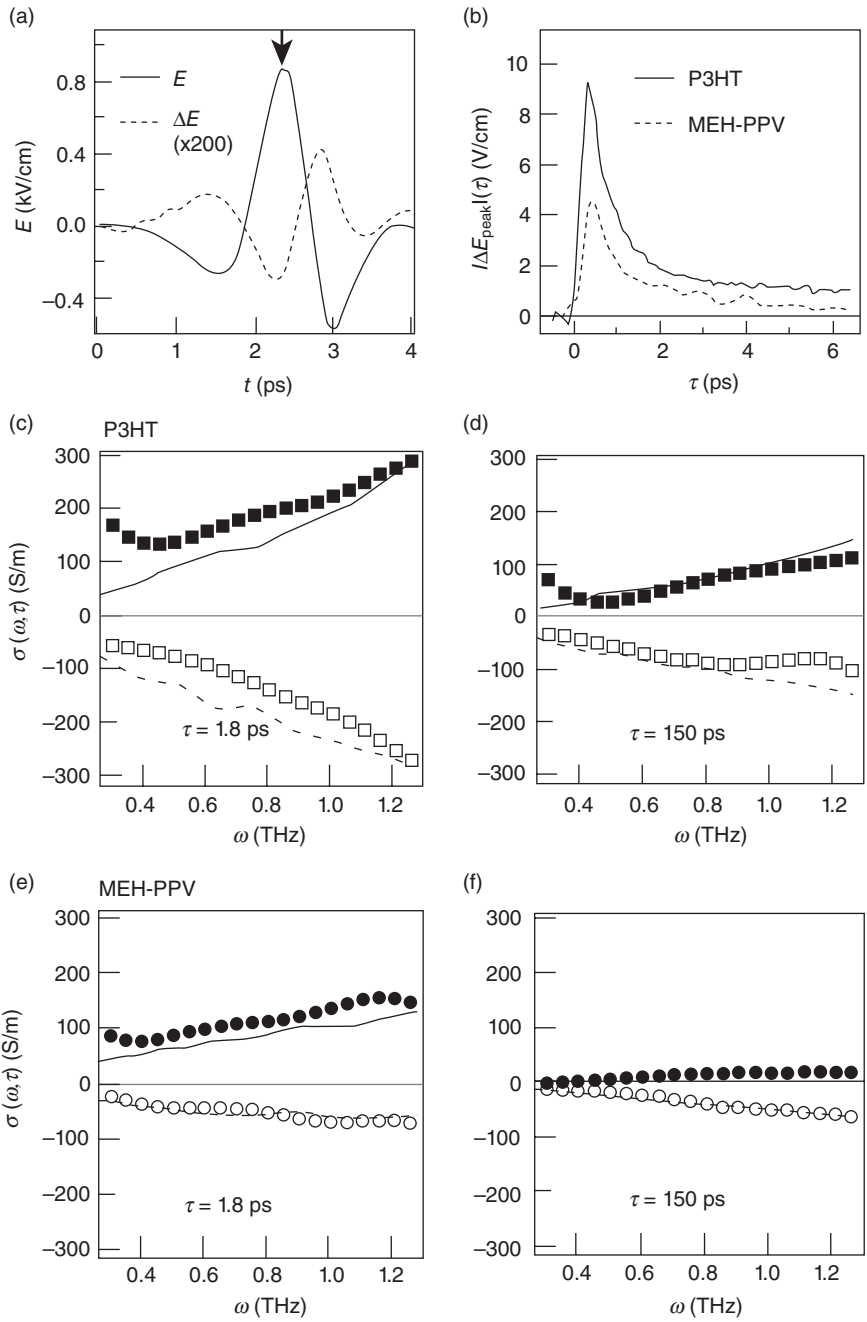

11.15 (a) The electric field $E(t)$ of the THz pulse transmitted through the rr-P3HT sample (solid line), with the modulation $\Delta E(t)$ measured 1 ps after photoexcitation (dotted line) and (b) decay of the modulation measured at the peak field strength. Real and imaginary conductivities for two different times: (c) and (d) rr-P3HT and (e) and (f) MEH-PPV (filled and open for real and imaginary parts respectively). The lines through the data points are to guide the eye. Adapted from Hendry, E., Koeberg, M., Schins, J. M., Siebbeles, L. D. A. & Bonn, M. 2006. Free carrier photogeneration in polythiophene versus poly(phenylene vinylene) studied with thz spectroscopy. *Chemical Physics Letters*, **432**, 441–445. Copyright (2006) with permission from Elsevier (DOI: 10.1016/j.cplett.2006.10.105).

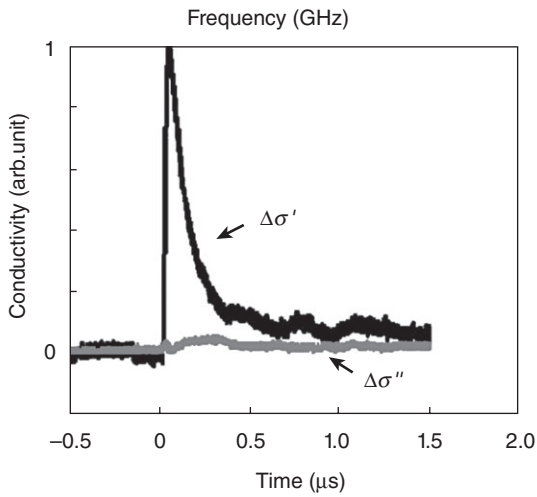

11.16 Normalized complex conductivity of a pentacene sample determined by microwave photoconductivity from analyzing transient Q-curve around 9 GHz center frequency. Reprinted with permission from Saeki, A., Seki, S. & Tagawa, S. 2006. Electrodeless measurement of charge carrier mobility in pentacene by microwave and optical spectroscopy techniques. *Journal of Applied Physics*, **100**, 023703, Copyright (2006), American Institute of Physics (DOI: 10.1063/1.2214638).

about 100 times higher than the 9 GHz Gunn oscillator frequency, hence THz spectroscopy using a few oscillations burst with THz bandwidth allows determining the complex conductivity on a larger frequency range.

In contrast, TPC spectroscopy probes the carrier mobility under DC bias since the electric field applied to the sample is essentially constant. The current density reads:

$$j = E\sigma + \varepsilon\frac{\mathrm{d}E}{\mathrm{d}t} + E\frac{\mathrm{d}\varepsilon}{\mathrm{d}t} \quad [11.5]$$

The temporal evolution of the carrier response currently accessible by the technique ranges from DC up to some 10 s of GHz. We emphasize that the technique does not probe any AC response.

The Drude Lorentz model suggests that stronger localization is detectable with higher probing frequency and that for each contributing oscillator, a certain range of frequency is needed to match it. The validation of more realistic carrier localization models involving potential barriers or wells can also benefit from experimental data over large ranges of frequency spaces, probing frequency and carrier evolution as function of pump-probe delay. A challenge is the disentanglement of both frequency spaces, since phenomena related to carrier evolution (generation, collection, recombination) may occur at same time or frequency scales as the ones due to localization. An approach to resolve this ambiguity consists in interpreting TRTS data in two-dimensional frequency space (Nemec *et al.*, 2009).

Therefore we emphasize the importance of combining different subnanosecond spectroscopic methods with specific sensitivity to charge carriers in order to span a wide range of probe frequencies and pump-probe delays, so that the cumulated spectral response allows matching the most adequate carrier dynamics model with the least assumptions.

11.7 Conclusion

To date, the nature of primary photoexcitation in organic crystals and polymers, and in particular the mechanisms of charge carrier photogeneration and transport are better understood, although some of their aspects remain controversial. As observed by several of the spectroscopic techniques presented here, the initial carrier photogeneration is independent of temperature, field, and wavelength, which is in contradiction with the predictions of the Onsager model (Moses *et al.*, 2001; Hegmann *et al.*, 2002). In bulk heterojunctions, photoconductivity observed by the relatively slow TRMC method does increase with temperature, however with low activation energies of tens of millielectronvolts (Savenije *et al.*, 2011; Murthy *et al.*, 2012). This has been attributed to thermal activation of detrapping from shallow traps.

In conjugated polymers, it is now accepted that a percentage of free carriers is generated directly (Moses *et al.*, 2002; Bakulin *et al.*, 2012) and that some polymer donor–acceptor blends reach high and even unitary internal quantum yield (Park *et al.*, 2009). For the remaining carriers that generate from secondary processes, electric-field assisted dissociation of excitons into polarons in about 10 ps has been reported

(Graupner *et al.*, 1998), and also excess excitation energy can possibly be involved in the hot-exciton dissociation process (Murthy *et al.*, 2012 and references therein).

More attention has been paid in recent years to establish relationships between structure/morphology and electronic/transport properties of organic semiconductors in view of organic photovoltaic applications. For instance, a recent time-resolved PIA study has shown that copolymers with different donor and acceptor moieties can acquire large yields of polaron pair formation. Enlarging the distance between center of masses of donor and acceptor can increase the recombination time of polaron pairs (Tautz *et al.*, 2012). The morphology of donor–acceptor blends, e.g. the degree of intercalation and the size of the crystalline domains, is also of paramount importance to achieve balanced electron and hole charge transport and carrier extraction (Rance *et al.*, 2011). It seems to be accepted that the transport in the lamellae of regioregular P3HT is somehow two-dimensional with a reduced 'Langevin' recombination rate as compared to the three-dimensional case. One approach consists of assuming monomolecular recombination and showing that bimolecular processes appear above a critical carrier density accounting for the sub-linear carrier density as function of excitation, and hence sub-linear evolution of observed TRMC (Dicker *et al.*, 2004) at a critical density that corresponds to more than one excitation per lamella. The other approach consists in deriving a bimolecular recombination coefficient for the two-dimensional case as suggested by Juška *et al.* (2009). This accounts for an overall 2.5 exponent power law of the recombination as function of carrier density. The overall behavior described by the two approaches is equivalent. The effect of dimensionality on charge transport properties is in agreement with the observation that thermal annealing and chemical additives that are known to increase donor–acceptor domain sizes induce higher charge carrier photogeneration and photovoltaic power conversion efficiencies (Ma *et al.*, 2005; Peet *et al.*, 2006).

Bimolecular recombination seems to become an important process when a solar cell is operated near open circuit (OC) voltage (Cowan *et al.*, 2012), although this point is still under debate (Deibel and Wagenpfahl, 2010; Street, 2010; Street and Schoendorf, 2010). The increase of recombination and hence the drop of photocurrent while approaching the OC voltage could then be responsible for the low fill factors of organic photovoltaic devices.

11.8 Acknowledgments

We gratefully acknowledge financial support from the CNRS-NTU-Thales UMI 3288 (CINTRA) and the NTU NAP startup Grant No. M4080511 as well as the Singapore Ministry of Education Academic Research Fund Tier 3 Grant No. MOE2011-T3-1-005.

11.9 References

Auston, D. H. 1975. Picosecond Optoelectronic Switching and Gating in Silicon. *Applied Physics Letters*, **26**, 101–103, DOI: 10.1063/1.88079.

Auston, D. H., Lavallard, P., Sol, N. & Kaplan, D. 1980. An Amorphous Silicon Photodetector for Picosecond Pulses. *Applied Physics Letters*, **36**, 66–68, DOI: 10.1063/1.91276.

Bakulin, A. A., Rao, A., Pavelyev, V. G., Van Loosdrecht, P. H. M., Pshenichnikov, M. S., Niedzialek, D., Cornil, J., Beljonne, D. & Friend, R. H. 2012. The Role of Driving Energy and Delocalized States for Charge Separation in Organic Semiconductors. *Science*, **335**, 1340–1344, DOI: 10.1126/science.1217745.

Bao, Z., Dodabalapur, A. & Lovinger, A. J. 1996. Soluble and Processable Regioregular Poly(3-Hexylthiophene) for Thin Film Field-Effect Transistor Applications with High Mobility. *Applied Physics Letters*, **69**, 4108, DOI: 10.1063/1.117834.

Beard, M. C., Turner, G. M. & Schmuttenmaer, C. A. 2000. Transient Photoconductivity in Gaas as Measured by Time-Resolved Terahertz Spectroscopy. *Physical Review B*, **62**, 15764–15777, DOI: 10.1103/PhysRevB.62.15764.

Brabec, C. J., Zerza, G., Cerullo, G., De Silvestri, S., Luzzati, S., Hummelen, J. C. & Sariciftci, S. 2001. Tracing Photoinduced Electron Transfer Process in Conjugated Polymer/Fullerene Bulk Heterojunctions in Real Time. *Chemical Physics Letters*, **340**, 232–236, DOI: 10.1016/s0009-2614(01)00431-6.

Brown, P. J., Sirringhaus, H., Harrison, M., Shkunov, M. & Friend, R. H. 2001. Optical Spectroscopy of Field-Induced Charge in Self-Organized High Mobility Poly(3-Hexylthiophene). *Physical Review B*, **63**, 125204, DOI: 10.1103/PhysRevB.63.125204.

Cowan, S. R., Banerji, N., Leong, W. L. & Heeger, A. J. 2012. Charge Formation, Recombination, and Sweep-out Dynamics in Organic Solar Cells. *Advanced Functional Materials*, **22**, 1116–1128, DOI: 10.1002/adfm.201101632.

Cunningham, P. D. & Hayden, L. M. 2008. Carrier Dynamics Resulting from above and Below Gap Excitation of P3ht and P3ht/Pcbm Investigated by Optical-Pump Terahertz-Probe Spectroscopy. *Journal of Physical Chemistry C*, **112**, 7928–7935, DOI: 10.1021/jp711827g.

De Haas, M. P. & Warman, J. M. 1982. Photon-Induced Molecular Charge Separation Studied by Nanosecond Time-Resolved Microwave Conductivity. *Chemical Physics*, **73**, 35–53, DOI: 10.1016/0301-0104(82)85148-3.

Deibel, C. & Wagenpfahl, A. 2010. Comment on 'Interface State Recombination in Organic Solar Cells'. *Physical Review B*, **82**, 207301, DOI: 10.1103/PhysRevB.82.207301.

Dicker, G., De Haas, M. P., Siebbeles, L. D. A. & Warman, J. M. 2004. Electrodeless Time-Resolved Microwave Conductivity Study of Charge-Carrier Photogeneration in Regioregular Poly(3-Hexylthiophene) Thin Films. *Physical Review B*, **70**, 045203, DOI: 10.1103/PhysRevB.70.045203.

Diesinger, H., Panahandeh-Fard, M., Baillargeat, D. & Soci, C. 2011. Electromagnetic Modeling and Optimization of Photoconductive Switches for Terahertz Generation and Photocurrent Transient Spectroscopy. *Proceedings of the 2011 IEEE MWP*, 373–376, DOI: 10.1109/MWP.2011.6088749.

Diesinger, H., Panahandeh-Fard, M., Wang, Z., Baillargeat, D. & Soci, C. 2012. Enhancing Photocurrent Transient Spectroscopy by Electromagnetic Modeling. *Review of Scientific Instruments*, **83**, 053103–6, DOI: 10.1063/1.4710996.

Ehrenfreund, E. & Vardeny, Z. V. 1997. Phonon Spectroscopy in Pi-Conjugated Polymers; the Role of the Excited Electronic States. *Optical Probes of Conjugated Polymers*, **3145**, 324–332, DOI: 10.1117/12.295532.

Fincher, C. R., JR., Ozaki, M., Heeger, A. J. & MacDiarmid, A. G. 1979. Donor and Acceptor States in Lightly Doped Polyacetylene, (Ch)_{X}. *Physical Review B*, **19**, 4140–4148, DOI: 10.1103/PhysRevB.19.4140.

Graupner, W., Cerullo, G., Lanzani, G., Nisoli, M., List, E. J. W., Leising, G. & De Silvestri, S. 1998. Direct Observation of Ultrafast Field-Induced Charge Generation in Ladder-Type Poly(Para-Phenylene). *Physical Review Letters*, **81**, 3259–3262, DOI: 10.1103/PhysRevLett.81.3259.

Green, K. & Sobolewski, R. 2000. Extending Scattering-Parameter Approach to Characterization of Linear Time-Varying Microwave Devices. *Microwave Theory and Techniques, IEEE Transactions on*, **48**, 1725–1731, DOI: 10.1109/22.873902.

Grzegorczyk, W. J., Savenije, T. J., Heeney, M., Tierney, S., McCulloch, I., Bavel, S. V. & Siebbeles, L. D. A. 2008. Relationship between Film Morphology, Optical, and Conductive Properties of Poly(Thienothiophene): [6,6]-Phenyl C-61-Butyric Acid Methyl Ester Bulk Heterojunctions. *The Journal of Physical Chemistry C*, **112**, 15973–15979, DOI: 10.1021/jp8044548.

Heeger, A. J., Sariciftci, N. S. & Namdas, E. B. 2010. *Semiconducting and Metallic Polymers*, New York, Oxford University Press.

Hegmann, F. A., Tykwinski, R. R., Lui, K. P. H., Bullock, J. E. & Anthony, J. E. 2002. Picosecond Transient Photoconductivity in Functionalized Pentacene Molecular Crystals Probed by Terahertz Pulse Spectroscopy. *Physical Review Letters*, **89**, 227403, DOI: 10.1103/PhysRevLett.89.227403.

Hegmann, F. A., Ostroverkhova, O., Gao, J. B., Barker, L., Tykwinski, R. R., Bullock, J. E., Anthony, J. E. 2004. Picosecond Transient Photoconductivity in Organic Molecular Crystals. *Ultrafast Phenomena in Semiconductors and Nonstructure Materials VIII*, **5352**, 196–207, DOI: 10.1117/12.526915.

Hendry, E., Koeberg, M., Schins, J. M., Siebbeles, L. D. A. & Bonn, M. 2006. Free Carrier Photogeneration in Polythiophene Versus Poly(Phenylene Vinylene) Studied with Thz Spectroscopy. *Chemical Physics Letters*, **432**, 441–445, DOI: 10.1016/j.cplett.2006.10.105.

Holt, J., Singh, S., Drori, T., Zhang, Y. & Vardeny, Z. V. 2009. Optical Probes of Pi-Conjugated Polymer Blends with Strong Acceptor Molecules. *Physical Review B*, **79**, 195210, DOI: 10.1103/PhysRevB.80.049902.

Holzman, J. F., Vermeulen, F. E., Arnold, B. W. & Elezzabi, A. Y. 2000. Photoconductive Gating of Picosecond Electrical Pulses on Thinned-Silicon Substrates. *Electronics Letters*, **36**, 1225–1226, DOI: 10.1049/el:20000895.

Horovitz, B. 1982. Infrared Activity of Peierls Systems and Application to Polyacetylene. *Solid State Communications*, **41**, 729–734, DOI: 10.1016/0038-1098(82)91126-7.

Infelta, P. P., De Haas, M. P. & Warman, J. M. 1977. The Study of the Transient Conductivity of Pulse Irradiated Dielectric Liquids on a Nanosecond Timescale Using Microwaves. *Radiation Physics and Chemistry*, **10**, 353–365, DOI: 10.1016/0146-5724(77)90044-9.

Juška, G., Genevičius, K., Nekrašas, N., Sliaužys, G. & Österbacka, R. 2009. Two Dimensional Langevin Recombination in Regioregular Poly(3-Hexylthiophene). *Applied Physics Letters*, **95**, 013303, DOI: 10.1063/1.3141513.

Ketchen, M. B., Grischkowsky, D., Chen, T. C., Chi, C. C., Duling, I. N., Halas, N. J., Halbout, J. M., Kash, J. A. & Li, G. P. 1986. Generation of Subpicosecond Electrical Pulses on Coplanar Transmission-Lines. *Applied Physics Letters*, **48**, 751–753, DOI: 10.1063/1.96709.

Kim, Y. H., Spiegel, D., Hotta, S. & Heeger, A. J. 1988. Photoexcitation and Doping Studies of Poly(3-Hexylthienylene). *Physical Review B*, **38**, 5490–5495, DOI: 10.1103/PhysRevB.38.5490.

Kraabel, B., Hummelen, J. C., Vacar, D., Moses, D., Sariciftci, N. S., Heeger, A. J. & Wudl, F. 1996. Subpicosecond Photoinduced Electron Transfer from Conjugated Polymers to Functionalized Fullerenes. *Journal of Chemical Physics*, **104**, 4267–4273, DOI: 10.1063/1.471154.

Lampin, J. F., Desplanque, L. & Mollot, F. 2001. Detection of Picosecond Electrical Pulses Using the Intrinsic Franz-Keldysh Effect. *Applied Physics Letters*, **78**, 4103–4105, DOI: 10.1063/1.1381030.

Lee, C. H., Yu, G., Moses, D., Pakbaz, K., Zhang, C., Sariciftci, N. S., Heeger, A. J. & Wudl, F. 1993. Sensitization of the Photoconductivity of Conducting Polymers by C-60 – Photoinduced Electron-Transfer. *Physical Review B*, **48**, 15425–15433, DOI: 10.1103/PhysRevB.48.15425.

Logeeswaran, V. J., Sarkar, A., Islam, M. S., Kobayashi, N. P., Straznicky, J., Li, X., Wu, W., Mathai, S., Tan, M. R. T., Wang, S.-Y. & Williams, R. S. 2008. A 14-Ps Full Width at Half Maximum High-Speed Photoconductor Fabricated with Intersecting Inp Nanowires on an Amorphous Surface. *Applied Physics A: Materials Science & Processing*, **91**, 1–5, DOI: 10.1007/s00339-007-4394-x.

Ma, W., Yang, C., Gong, X., Lee, K. & Heeger, A. J. 2005. Thermally Stable, Efficient Polymer Solar Cells with Nanoscale Control of the Interpenetrating Network Morphology. *Advanced Functional Materials*, **15**, 1617–1622, DOI: 10.1002/adfm.200500211.

Miranda, P. B., Moses, D. & Heeger, A. J. 2001. Ultrafast Photogeneration of Charged Polarons in Conjugated Polymers. *Physical Review B*, **64**, 081201(R), DOI: 10.1103/PhysRevB.64.081201.

Mizrahi, U., Shtrichman, I., Gershoni, D., Ehrenfreund, E. & Vardeny, Z. V. 1999. Picoseconds Time Resolved Photoinduced Absorption by Infrared Active Vibrations as a Probe for Charge Photogeneration in Meh-Ppv/C-60 Composites. *Synthetic Metals*, **102**, 1182–1185, DOI: 10.1016/s0379-6779(98)00316-6.

Moses, D., Sinclair, M. & Heeger, A. J. 1987. Carrier Photogeneration and Mobility in Polydiacetylene – Fast Transient Photoconductivity. *Physical Review Letters*, **58**, 2710–2713, DOI: 10.1103/PhysRevLett.58.2710.

Moses, D., Sinclair, M., Phillips, S. & Heeger, A. J. 1989. Transient Photoconductivity in Polyacetylene and Polydiacetylene. *Synthetic Metals*, **28**, D675–D681, DOI: 10.1016/0379-6779(89)90760-1.

Moses, D., Dogariu, A. & Heeger, A. J. 2000. Ultrafast Detection of Charged Photocarriers in Conjugated Polymers. *Physical Review B*, **61**, 9373–9379, DOI: 10.1103/PhysRevB.61.9373.

Moses, D., Soci, C., Miranda, P. & Heeger, A. J. 2001. The Role of Electron Photoemission in the 'Photoconductivity' of Semiconducting Polymers. *Chemical Physics Letters*, **350**, 531–536, DOI: 10.1016/S0009-2614(01)01317-3.

Moses, D., Miranda, P. B., Soci, C. & Heeger, A. J. 2002. Mechanism of Carrier Photoexcitation in Semiconducting Polymers: The Role of Electron Photoemission in 'Photoconductivity' Measurements. In: Jabbour, G. E. & Sariciftci, N. S. (eds.)

Electronic, Optical and Optoelectronic Polymers and Oligomers. Warrendale: Materials Research Society, DOI: 10.1117/12.456939.

Moses, D., Soci, C., Chi, X. L. & Ramirez, A. P. 2006. Mechanism of Carrier Photogeneration and Carrier Transport in Molecular Crystal Tetracene. *Physical Review Letters*, **97**, 067401-067404, DOI: 10.1103/PhysRevLett.97.067401.

Mourou, G. A. & Meyer, K. E. 1984. Subpicosecond Electro-Optic Sampling Using Coplanar Strip Transmission-Lines. *Applied Physics Letters*, **45**, 492–494, DOI: 10.1063/1.95312.

Murthy, D. H. K., Gao, M., Vermeulen, M. J. W., Siebbeles, L. D. A. & Savenije, T. J. 2012. Mechanism of Mobile Charge Carrier Generation in Blends of Conjugated Polymers and Fullerenes: Significance of Charge Delocalization and Excess Free Energy. *The Journal of Physical Chemistry C*, **116**, 9214–9220, DOI: 10.1021/jp3007014.

Nemec, H., Nienhuys, H. K., Perzon, E., Zhang, F. L., Inganas, O., Kuzel, P. & Sundstrom, V. 2009. Ultrafast Conductivity in a Low-Band-Gap Polyphenylene and Fullerene Blend Studied by Terahertz Spectroscopy. *Physical Review B*, **79**, 245326, DOI: 10.1103/Physrevb.79.245326.

Osterbacka, R., An, C. P., Jiang, X. M. & Vardeny, Z. V. 2000. Two-Dimensional Electronic Excitations in Self-Assembled Conjugated Polymer Nanocrystals. *Science*, **287**, 839–842, DOI: 10.1126/science.287.5454.839.

Osterbacka, R., Pivrikas, A., Juska, G., Poskus, A., Aarnio, H., Sliaužys, G., Genevičius, K., Arlauskas, K. & Sariciftci, N. S. 2010. Effect of 2-D Delocalization on Charge Transport and Recombination in Bulk-Heterojunction Solar Cells. *IEEE Journal of Selected Topics in Quantum Electronics*, **16**, 1738–1745, DOI: 10.1109/JSTQE.2010.2048746.

Ostroverkhova, O., Cooke, D. G., Shcherbyna, S., Egerton, R. F., Hegmann, F. A., Tykwinski, R. R. & Anthony, J. E. 2005a. Bandlike Transport in Pentacene and Functionalized Pentacene Thin Films Revealed by Subpicosecond Transient Photoconductivity Measurements. *Physical Review B*, **71**, 035204, DOI: 10.1103/Physrevb.71.035204.

Ostroverkhova, O., Shcherbyna, S., Cooke, D. G., Egerton, R. F., Hegmann, F. A., Tykwinski, R. R., Parkin, S. R. & Anthony, J. E. 2005b. Optical and Transient Photoconductive Properties of Pentacene and Functionalized Pentacene Thin Films: Dependence on Film Morphology. *Journal of Applied Physics*, **98**, 033701, DOI: 10.1063/1.1949711.

Ostroverkhova, O., Cooke, D. G., Hegmann, F. A., Anthony, J. E., Podzorov, V., Gershenson, M. E., Jurchescu, O. D. & Palstra, T. T. M. 2006. Ultrafast Carrier Dynamics in Pentacene, Functionalized Pentacene, Tetracene, and Rubrene Single Crystals. *Applied Physics Letters*, **88**, 162101, DOI: 10.1063/1.2193801.

Park, S. H., Roy, A., Beaupre, S., Cho, S., Coates, N., Moon, J. S., Moses, D., Leclerc, M., Lee, K. & Heeger, A. J. 2009. Bulk Heterojunction Solar Cells with Internal Quantum Efficiency Approaching 100%. *Nature Photonics*, **3**, 297–302, DOI: 10.1038/nphoton.2009.69.

Parkinson, P., Lloyd-Hughes, J., Gao, Q., Tan, H. H., Jagadish, C., Johnston, M. B. & Herz, L. M. 2007. Transient Terahertz Conductivity of GaAs Nanowires. *Nano Letters*, **7**, 2162–2165, DOI: 10.1021/nl071162x.

Peet, J., Soci, C., Coffin, R. C., Nguyen, T. Q., Mikhailovsky, A., Moses, D. & Bazan, G. C. 2006. Method for Increasing the Photoconductive Response in Conjugated

Polymer/Fullerene Composites. *Applied Physics Letters*, **89**, 252105–3, DOI: 10.1063/1.2408661.

Prins, P., Grozema, F. C., Schins, J. M., Savenije, T. J., Patil, S., Scherf, U. & Siebbeles, L. D. A. 2006. Effect of Intermolecular Disorder on the Intrachain Charge Transport in Ladder-Type Poly(p-Phenylenes). *Physical Review B*, **73**, 045204, DOI: 10.1103/PhysRevB.73.045204.

Rance, W. L., Ferguson, A. J., McCarthy-Ward, T., Heeney, M., Ginley, D. S., Olson, D. C., Rumbles, G. & Kopidakis, N. 2011. Photoinduced Carrier Generation and Decay Dynamics in Intercalated and Non-Intercalated Polymer:Fullerene Bulk Heterojunctions. *ACS Nano*, **5**, 5635–5646, DOI: 10.1021/nn201251v.

Saeki, A., Seki, S. & Tagawa, S. 2006. Electrodeless Measurement of Charge Carrier Mobility in Pentacene by Microwave and Optical Spectroscopy Techniques. *Journal of Applied Physics*, **100**, 023703, DOI: 10.1063/1.2214638.

Sariciftci, N. S. 1997. *Primary Photoexcitations in Conjugated Polymers: Molecular Exciton Versus Semiconductor Band Model*, Singapore, World Scientific Publishing Co.

Sariciftci, N. S. & Heeger, A. J. 1994. Reversible, Metastable, Ultrafast Photoinduced Electron-Transfer in Conjugated Polymer and Buckminsterfullerene Composites and Heterojunctions. *Molecular Crystals and Liquid Crystals Science and Technology Section A – Molecular Crystals and Liquid Crystals*, **256**, 317–326, DOI: 10.1080/10587259408039262.

Sariciftci, N. S., Smilowitz, L., Heeger, A. J. & Wudl, F. 1992. Photoinduced Electron-Transfer from a Conducting Polymer to Buckminsterfullerene. *Science*, **258**, 1474–1476, DOI: 10.1126/science.258.5087.1474.

Savenije, T. J., Murthy, D. H. K., Gunz, M., Gorenflot, J., Siebbeles, L. D. A., Dyakonov, V. & Deibel, C. 2011. Absence of Postnanosecond Charge Carrier Relaxation in Poly(3-Hexylthiophene)/Fullerene Blends. *The Journal of Physical Chemistry Letters*, **2**, 1368–1371, DOI: 10.1021/jz200569h.

Schaffer, H. E., Friend, R. H. & Heeger, A. J. 1987. Localized Phonons Associated with Solitons in Polyacetylene – Coupling to the Nonuniform Mode. *Physical Review B*, **36**, 7537–7541, DOI: 10.1103/PhysRevB.36.7537.

Sirringhaus, H., Tessler, N. & Friend, R. H. 1998. Integrated Optoelectronic Devices Based on Conjugated Polymers. *Science*, **280**, 1741–1744, DOI: 10.1126/science.280.5370.1741.

Sirringhaus, H., Brown, P. J., Friend, R. H., Nielsen, M. M., Bechgaard, K., Langeveld-Voss, B. M. W., Spiering, A. J. H., Janssen, R. A. J., Meijer, E. W., Herwig, P. & de Leeuw, D. M. 1999. Two-Dimensional Charge Transport in Self-Organized, High-Mobility Conjugated Polymers. *Nature*, **401**, 685–688, DOI: 10.1038/44359.

Smith, F. W., Q. Le, H., Diadiuk, V., Hollis, M. A., Calawa, A. R., Gupta, S., Frankel, M., Dykaar, D. R., Mourou, G. A. & Hsiang, T. Y. 1989. Picosecond Gaas-Based Photoconductive Optoelectronic Detectors. *Applied Physics Letters*, **54**, 890–892, DOI: 10.1063/1.100800.

Smith, N. V. 2001. Classical Generalization of the Drude Formula for the Optical Conductivity. *Physical Review B*, **64**, 155106, DOI: 10.1103/PhysRevB.64.155106.

Smith, P. R., Auston, D. H., Johnson, A. M. & Augustyniak, W. M. 1981. Picosecond Photoconductivity in Radiation-Damaged Silicon-on-Sapphire Films. *Applied Physics Letters*, **38**, 47–50, DOI: 10.1063/1.92128.

Soci, C., Moses, D., Xu, Q. H. & Heeger, A. J. 2005. Charge-Carrier Relaxation Dynamics in Highly Ordered Poly(P-Phenylene Vinylene): Effects of Carrier

Bimolecular Recombination and Trapping. *Physical Review B*, **72**, 5204, DOI: 10.1103/PhysRevB.72.245204.

Soci, C., Hwang, I. W., Moses, D., Zhu, Z., Waller, D., Gaudiana, R., Brabec, C. J. & Heeger, A. J. 2007. Photoconductivity of a Low-Bandgap Conjugated Polymer. *Advanced Functional Materials*, **17**, 632–636, DOI: 10.1002/adfm.200600199.

Soos, Z. G., Hayden, G. W., Girlando, A. & Painelli, A. 1994. Pariser-Parr-Pople Force Field for π-Electrons – Raman and Infrared Shifts of Transpolyacetylene. *Journal of Chemical Physics*, **100**, 7144–7152.

Street, R. 2010. Reply to 'Comment on "Interface State Recombination in Organic Solar Cells" '. *Physical Review B*, **82**, DOI: 10.1103/PhysRevB.82.207302.

Street, R. A. & Schoendorf, M. 2010. Interface State Recombination in Organic Solar Cells. *Physical Review B*, **81**, DOI: 10.1103/PhysRevB.81.205307.

Tautz, R., Da Como, E., Limmer, T., Feldmann, J., Egelhaaf, H.-J., Von Hauff, E., Lemaur, V., Beljonne, D., Yilmaz, S., Dumsch, I., Allard, S. & Scherf, U. 2012. Structural Correlations in the Generation of Polaron Pairs in Low-Bandgap Polymers for Photovoltaics. Nature Communications, **3**, 970, DOI: 10.1038/ncomms1967.

Thorsmolle, V. K., Averitt, R. D., Chi, X., Hilton, D. J., Smith, D. L., Ramirez, A. P. & Taylor, A. J. 2004. Ultrafast Conductivity Dynamics in Pentacene Probed Using Terahertz Spectroscopy. *Applied Physics Letters*, **84**, 891–893, DOI: 10.1063/1.1644046.

Tripon-Canseliet, C., Faci, S., Blary, K., Deshours, F., Alquie, G., Formont, S. & Chazelas, J. 2006. Optically-Controlled Microwave Phase Shifting and Sampling by Efficient Photoconductive Switching on Lt-Gaas Substrate Integrated Technology. *Proceedings of the Society of Photooptical Instrumentation Engineers (SPIE)*, 6343, Photonics North 2006, 63432K, DOI: 10.117/12,707688.

Ulbricht, R., Hendry, E., Shan, J., Heinz, T. F. & Bonn, M. 2011. Carrier Dynamics in Semiconductors Studied with Time-Resolved Terahertz Spectroscopy. *Reviews of Modern Physics*, **83**, 543–586, DOI: 10.1103/RevModPhys.83.543.

Unuma, T., Fujii, K., Kishida, H. & Nakamura, A. 2010. Terahertz Complex Conductivities of Carriers with Partial Localization in Doped Polythiophenes. *Applied Physics Letters*, **97**, 03308, 1–3, DOI: 10.1063/1.3466916.

Valdmanis, J., Mourou, G. & Gabel, C. 1983. Subpicosecond Electrical Sampling. *IEEE Journal of Quantum Electronics*, **19**, 664–667, DOI: 10.1109/jqe.1983.1071915.

Valdmanis, J. A., Mourou, G. & Gabel, C. W. 1982. Picosecond Electro-Optic Sampling System. *Applied Physics Letters*, **41**, 211–212, DOI: 10.1063/1.93485.

Voss, K. F., Foster, C. M., Smilowitz, L., Mihailovic, D., Askari, S., Srdanov, G., Ni, Z., Shi, S., Heeger, A. J. & Wudl, F. 1991. Substitution Effects on Bipolarons in Alkoxy Derivatives of Poly(1,4-Phenylene-Vinylene). *Physical Review B*, **43**, 5109–5118, DOI: 10.1103/PhysRevB.43.5109.